HHS Public Access

Author manuscript

Nat Microbiol. Author manuscript; available in PMC 2020 March 16.

Published in final edited form as:

Nat Microbiol. 2019 December ; 4(12): 2523–2537. doi:10.1038/s41564-019-0551-1.

Enterovirus Pathogenesis Requires the Host Methyltransferase SETD3

Jonathan Diep[1,*], **Yaw Shin Ooi**[1,*], **Alex W. Wilkinson**[2,*], **Christine E. Peters**[1], **Eileen Foy**[3], **Jeffrey R. Johnson**[4], **James Zengel**[1], **Siyuan Ding**[1,6,7], **Kuo-Feng Weng**[1], **Orly Laufman**[3], **Gwendolyn Jang**[4], **Jiewei Xu**[4], **Tracy Young**[4], **Erik Verschueren**[4], **Kristi J. Kobluk**[1], **Joshua E. Elias**[5], **Peter Sarnow**[1], **Harry B. Greenberg**[1,6,7], **Ruth Hüttenhain**[4], **Claude M. Nagamine**[8], **Raul Andino**[3,§], **Nevan J. Krogan**[4,§], **Or Gozani**[2,§], **Jan E. Carette**[1,9,§]

[1] -Department of Microbiology and Immunology, Stanford University School of Medicine, 299 Campus Drive, Stanford, CA 94305

[2] -Department of Biology, Stanford University, 327 Campus Drive, Stanford, California 94305, USA

[3] -Department of Microbiology and Immunology, University of California, San Francisco, 600 16th Street, San Francisco, CA 94158

[4] -Department of Cellular Molecular Pharmacology, University of California, San Francisco, 1700 4th Street, San Francisco, CA 94158

[5] -Chan Zuckerberg Biohub, Mass Spectrometry Platform, Stanford CA 94305, USA

[6] -Department of Medicine, Division of Gastroenterology and Hepatology, Stanford University, 300 Pasteur Drive, Stanford, CA 94305, USA

[7] -Palo Alto Veterans Institute of Research, VA Palo Alto Health Care System, Palo Alto, CA 94304, USA

[8] -Department of Comparative Medicine, Stanford University School of Medicine, 287 Campus Drive, Stanford, CA 94305

[9] -Lead contact

Abstract

§ -Correspondence to: carette@stanford.edu, ogozani@stanford.edu, nevan.krogan@gladstone.ucsf.edu, or raul.andino@ucsf.edu.

Author contributions:

J.D., Y.S.O., and A.W.W. were responsible for design and execution of experiments, data analysis, and manuscript preparation. C.E.P. analyzed & generated phylogenetic tree of SET domain family members, performed CV-B3 2A alanine scan, and analyzed 3-dimensional structure of SETD3-binding mutants of 2A. E.F., J.R.J., O.L., G.J., T.Y., E.V., R.A. and N.J.K designed, collected and analyzed the CV-B3 virus-host interaction proteomics data and A.W.W. performed and analyzed actin methylation mass spectrometry experiments with help from J.E.E. J.Z. performed statistical analyses for all datasets as well as cloned and analyzed GFP-ΔVP1-2A constructs and CV-B3 infectious clones that harbor SETD3-binding mutants of 2A. R.H., G.J., J.X. and N.J.K. designed, collected and analyzed the multiple enteroviruses' 2A AP-MS datasets. C.M.N., K.F.W., J.D., K.J.K. and P.S. were responsible for *in vivo* mice experiments and analysis. S.D. and H.B.G. were responsible for examining innate immune responses and expression levels of ISGs by transcriptome-wide RNA sequencing. J.E.C, O.G., N.J.K. and R.A. supervised the research, interpreted data and prepared the manuscript.

* -Contributed equally to this work

Competing Interests:

The authors declare competing financial interests: O.G. is a co-founder of EpiCypher, Inc. and Athelas Therapeutics, Inc.

Enteroviruses (EVs) comprise a large genus of positive-sense, single-stranded RNA viruses whose members cause a number of important and widespread human diseases including poliomyelitis, myocarditis, acute flaccid myelitis (AFM) and the common cold. How EVs co-opt cellular functions to promote replication and spread is incompletely understood. Here, using genome-scale CRISPR screens, we identify the actin histidine methyltransferase SETD3 as critically important for viral infection by a broad panel of enteroviruses including rhinoviruses and non-polio EVs increasingly linked to severe neurological disease such as AFM (EV-D68) and viral encephalitis (EV-A71). We show that cytosolic SETD3, independent of its methylation activity, is required for the RNA replication step in the viral life cycle. Using quantitative affinity purification-mass spectrometry, we show that SETD3 specifically interacts with the viral 2A protease of multiple enteroviral species and we map the residues in 2A that mediate this interaction. 2A mutants that retain protease activity, but unable to interact with SETD3, are severely compromised in RNA replication. These data suggest a role of the viral 2A protein in RNA replication beyond facilitating proteolytic cleavage. Finally, we demonstrate that SETD3 is essential for *in vivo* replication and pathogenesis in multiple mouse models for enterovirus infection including CV-A10, EV-A71 and EV-D68. Our results reveal a crucial role of a host protein in viral pathogenesis and suggest targeting SETD3 as a potential mechanism for controlling viral infections.

Host-directed therapy (HDT) is an emerging approach in the field of antivirals[1]. The strategy behind HDT is to interfere with host cell proteins required for viral infection. Respiratory enteroviruses (EVs) are an attractive target for the development of HDT. For example, rhinovirus infection is widespread, has an enormous economic cost[2] and is a major cause of severe asthma exacerbations[3]. The remarkable phenotypic diversity[4] has precluded development of a vaccine and effective antivirals. In addition, some non-polio enteroviruses such as EV-D68[5] can cause recurrent outbreaks and are probable causes of acute flaccid myelitis, a paralyzing disease resembling poliomyelitis[5].

Results

To identify common mechanisms by which the enteroviruses hijack the cellular machinery to promote replication and spread, we performed genome-wide CRISPR-Cas9 screens with recently isolated strains of respiratory enteroviruses. We chose rhinovirus C (RV-C15), a virus species linked to severe childhood asthma, and the more distantly related enterovirus EV-D68. To create a cell line susceptible to RV-C15 infection we stably expressed CDHR3, the cellular receptor for type C rhinoviruses[6], in H1-HeLa cells (Supplementary Fig. 1a, 1b). This cell line, named H1-HeLa^{+CHDR3}, supports replication of both RV-C15 and EV-D68. After mutagenesis with a genome-scale CRISPR-Cas9 knockout library[7], cells were infected in parallel with either RV-C15 or EV-D68 (Missouri 2014 outbreak strain; EV-D68 MO) (Fig. 1a). To identify gene mutations that protect against viral infection, we retrieved the guide RNA (gRNA) sequences present in the resistant population and compared it to the unselected population. Using the MAGeCK algorithm[8] we found strong enrichment of gRNAs targeting known entry receptors for both viruses, i.e. CDHR3 for RV-C15[6] and sialic acid biosynthesis genes for EV-D68[9] (Supplementary Fig. 2a, 2b and Supplementary Table 1). In a comparative analysis, we found *CSDE1*, *PLA2G16* and *SETD3* to be critically required for both enteroviruses (Fig. 1b and Supplementary Table 1). *CSDE1* and *PLA2G16*

have previously described roles in enterovirus infections[10,11], highlighting the robustness of our genetic screens. Strikingly, the recently identified histidine methyltransferase *SETD3*[12,13] was the single most enriched gene shared by both viruses.

We first sought to directly test SETD3 as a host factor essential for RV-C15 and EV-D68 infection by creating an isogenic knockout cell line of SETD3 ($SETD3^{KO}$) in H1-HeLa $^{+CDHR3}$ cells using CRISPR-Cas9 gene-editing (Supplementary Fig. 3a, 3b). In time course infection assays, SETD3 deficiency resulted in severe replication defects for RV-C15 and EV-D68 MO, which could be rescued by complementation with a wild-type copy of *SETD3* using lentiviral transduction (Fig. 1c, 1d). Challenging $SETD3^{KO}$ cells with representative members from all three rhinovirus species (A, B and C) and with EV-D68 2014 outbreak[14] strains resulted in an equally severe (>1,000-fold) reduction in viral RNA accumulation at 16 hours post-infection (hpi) (Fig. 1e, 1f). Rhinoviruses and EV-D68 are picornaviruses that belong to the genus *Enterovirus,* which comprises at least 7 known species of human enteroviruses (Fig. 1g, top panel). We found that SETD3 deficiency resulted in a strong resistance to viral infection by representative members of each human enterovirus species, e.g. coxsackievirus A10 (CV-A10), coxsackievirus B3 (CV-B3), poliovirus (PV-1), EV-D68 and rhinoviruses. Consistent with resistance to viral infection, $SETD3^{KO}$ cells were protected against the cytopathic effects observed in wild-type (WT) cells and SETD3 complemented cells (Fig. 1g, bottom panel). In line with these results, SETD3 was previously identified in a genetic screen for CV-A7 infection[11], but was not further validated in the study. Interestingly, the role of SETD3 did not extend to the whole *Picornaviridae* family as encephalomyocarditis virus (EMCV), a cardiovirus, was unaffected by SETD3 knockout ($SETD3^{KO}$) (Fig. 1g). Additionally, SETD3 was dispensable for several other, disparate RNA viruses that are members of the families *Togaviridae*, *Rhabdoviridae* and *Flaviviridae* (Supplementary Fig. 4). Thus, SETD3 is an essential host factor that is broadly required for infection by viruses from the human enterovirus genus.

SETD3 belongs to a class of protein methyltransferases containing the catalytic SET domain that has recently been linked to antiviral immunity mediated by interferon (IFN)[15,16]. Thus, to determine if the mechanism of action of viral resistance in $SETD3^{KO}$ cells is through an upregulation of IFN-stimulated genes (ISGs), we first performed transcriptome-wide RNA sequencing in uninfected WT and $SETD3^{KO}$ cells. $SETD3^{KO}$ cells did not upregulate a core set of ISGs compared to WT cells (Supplementary Table 2). Moreover, no differences were observed in innate immune activation when challenged with different enteroviruses or treated with IFN-β suggesting that the reduction in viral RNA accumulation levels observed in $SETD3^{KO}$ cells is not through IFN signaling (Supplementary Fig. 5). To gain more mechanistic insight into SETD3 we sought to determine which stage of the viral life cycle SETD3 acts. We first interrogated the translation and replication step of the life cycle by electroporating the RNA of a RV-B14 replicon into cells, bypassing the entry route. In contrast to WT cells in which we observed a strong luciferase signal due to active viral replication at 24 hours post-electroporation, the luciferase signal in $SETD3^{KO}$ did not exceed the background levels observed in mock-electroporated cells (Fig. 2a, left panel). This was not because $SETD3^{KO}$ cells do not support electroporation or have a general defect in host metabolism as we observed no differences in luciferase accumulation when capped luciferase mRNA was electroporated (Fig. 2a, right panel). The strong defect observed in

viral replication even when normal entry was bypassed suggests that SETD3 has a role after entry and uncoating of enteroviruses, perhaps during the subsequent steps of the infection cycle, i.e. viral protein translation and genome replication in the cytoplasm. To further investigate this, we performed synchronized infection assays using an infectious CV-B3 virus encoding luciferase (CV-B3-RLuc). Infection of wild-type cells led to an initial period (≤ 3 hpi) of translation of the incoming viral genome, which was inhibited with the translation inhibitor cycloheximide but not with guanidine hydrochloride (GuHCl), a potent inhibitor of viral replication. A subsequent period (> 3 hpi) of exponential increase of luciferase signal was observed due to the amplification of the viral genome, which was inhibited by GuHCl. In SETD3-deficient cells, untreated or treated with GuHCl, we observed no major defect in initial translation, but a severe decrease in luciferase signal later in infection, suggesting that SETD3 is important for viral genome replication (Fig. 2b).

SETD3 was localized predominantly in the cytosol (Fig. 2c). To further examine the necessity of cytosolic localization of SETD3 for its role in viral replication, we introduced dominant localization signals to SETD3. In the SETD3^{KO} cell background, we re-localized SETD3 exclusively to either the nucleus using a nuclear import signal (NLS) or the cytoplasm using a nuclear export signal (NES) and stably expressed the localization mutants under a minimal promoter to avoid potential artifacts due to overexpression (Fig. 2c and Supplementary Fig. 6). When challenged with RV-C15 or EV-D68, only the cytoplasm-localized SETD3 rescued viral infection equivalent to that of the wild-type complement (Fig. 2d). This result is consistent with the importance of SETD3 for viral replication, which occurs in the cytoplasm of the host cell.

Among SET domain lysine methyltransferases, SETD3 clusters with SETD4 and SETD6, which are unique in that they share a Rubisco-substrate binding (RSB) domain homologous to plant Rubisco LSMT (Large subunit methyltransferase) (Supplementary Fig. 7a and Fig. 3a, top panel). To determine whether other members of the human RSB-containing group can functionally complement SETD3, SETD3^{KO} cells were stably transduced to express either SETD4 or SETD6 (Supplementary Fig. 7b) and challenged with RV-C15 or EV-D68. For both viruses, only SETD3 rescued viral infection, suggesting there was no functional redundancy despite having similar conserved domains (Supplementary Fig. 7c). The difference could be due to substrate preference, protein structure, or subcellular localization (Supplementary Fig. 7d). Recently, SETD3 was identified as the first known metazoan protein histidine methyltransferase and the enzyme responsible for generating the abundant methyl modification on actin histidine 73 (H73), emphasizing its uniqueness amongst the protein methyltransferases[12,13]. To gain insight into the SETD3 domains required for viral infection, we generated a panel of C-terminal truncation mutants. These mutants were first tested for *in vitro* methylation activity on actin. Actin methylation activity was detected only when both the SET domain and RSB-domain were intact (Fig. 3a). The truncation mutants (SETD3$^{1-492}$, SETD3$^{1-527}$, and SETD3$^{1-563}$) with intact SET and RSB domains not only rescued actin methylation activity but also supported RV-C15 and EV-D68 MO infection (Fig. 3b). Complementation with the RSB domain alone could not rescue viral replication (Supplementary Fig. 8a, 8b). Thus, both the SET-domain and RSB-domains of SETD3 are important for viral infection.

To determine whether the catalytic activity of SETD3 is required for the role of SETD3 in enterovirus replication, we constructed a catalytically inactive SETD3 mutant (named SETD3-5M) by introducing 5 mutations in conserved residues that participate in forming the active-site pocket for actin methylation[12] (W274, Y313, and R316) and conserved residues important for S-adenosyl methionine (SAM, the methyl donor for methyltransferases) binding (N278, H279). Although actin is the only known, bona fide substrate for SETD3, the same mutations are predicted to abolish methylation of any unknown substrates of the methyltransferase. In wild-type cells, almost all actin was methylated at His73 (>95%) whereas in SETD3^{KO} cells the His73 methylation was undetected (Fig. 3c). Stable expression of wild type SETD3 cDNA restored actin methylation in the SETD3^{KO} cells, whereas expression of the SETD3-5M mutant was unable to restore actin methylation (Fig. 3c). Strikingly, despite undetectable levels of methylated actin in cells stably complemented with the SETD3-5M mutant, viral replication of RV-C15 and EV-D68 was restored to comparable levels as in cells expressing wild-type SETD3 (Fig, 3d). Similar results were obtained upon SETD3-5M complementation using a promoter that drives lower levels of expression (Supplementary Fig. 8c, 8d, 8e, 8f). Thus, SETD3 promotes viral replication through the SET and RSB domains, but without a requirement *per se* for the methylation activity.

To gain more mechanistic insight into how SETD3 engages with enteroviral replication, we adopted an unbiased proteomic approach. To systematically and comprehensively identify viral-host interacting proteins, all CV-B3 viral proteins were fused to a Strep-affinity tag and expressed individually in 293T cells (Supplementary Fig. 9 and Supplementary Fig. 10a). Expression of catalytically active 2A (2A^{WT}) protease cleaves multiple cellular proteins (e.g. NUP98 and EIF4G1) leading to host translation shutoff and cell toxicity[17]. Therefore, all enterovirus 2A constructs that we used in this report are catalytically inactive mutants, unless otherwise stated. Specifically, we used a CV-B3 2A mutant that encodes a substitution of the active-site cysteine (2A^{C107A}). The viral proteins were affinity purified and interacting host proteins were identified by mass spectrometry (MS) (Supplementary Fig. 9 and Supplementary Fig. 10a). Using a specialized scoring system for host-virus interactions termed MiST[18], which takes into account peptide abundance, reproducibility and specificity, we identified 170 cellular proteins that interact robustly (MiST score ≥0.75) with enteroviral proteins (Supplementary Table 4). Amongst this core set multiple, well-studied and validated interactions were present including NUP98[19] and IF4G1 (*EIF4G1*)[20] interactions with 2A and GCP60 (*ACBD3*)[21], GBF1[22], and PI4KB[21] interactions with 3A (Supplementary Fig. 10b and Supplementary Table 4). Importantly, using this unbiased method, SETD3 was identified specifically in the 2A pull-down, suggesting that SETD3 interacts with the viral 2A protease (Supplementary Fig. 10b, 10c, and Fig. 4a). In line with the observation that SETD3 methyltransferase activity is not required for its role in viral replication, we found that 2A is not methylated by SETD3 in an *in vitro* methylation assay (Supplementary Fig. 11). We confirmed the 2A-SETD3 interaction by co-transfection of FLAG-SETD3 and CV-B3 2A-Strep followed by immunoprecipitation of FLAG-SETD3 and western blotting. In this reciprocal pull-down, we found that CV-B3 2A co-purified with SETD3, but not the unrelated 2A of EMCV (Fig. 4b). Consistent with the analysis of SETD3 truncation mutants (Fig. 3a and 3b), the largest SETD3 truncation mutant

(SETD3$^{1-453}$) that did not rescue virus infection also lost its ability to pull down 2A, whereas the smallest SETD3 truncation mutant (SETD3$^{1-492}$) that rescued virus infection did pull down 2A (Supplementary Fig. 12). We further examined the interaction of SETD3 with viral proteins during enteroviral infection. For this, we generated a cell line that stably expresses SETD3 fused to a dual affinity purification tag[23]. After infection with CV-A10, a causative agent for hand-foot-and-mouth disease, cell lysates were subjected to tandem-affinity immunoprecipitation and subsequent MS analysis (Supplementary Fig. 13a, Supplementary Table 3). Of the viral proteins that were recovered in the SETD3 pull down (n = 1), the 2A viral protease represented ~76% of total viral peptides recovered (Supplementary Fig. 13b, Supplementary Table 3). These data suggest that the 2A-SETD3 interaction is not limited to a single enterovirus species. To more broadly assess the generality of this interaction, we expressed 2A proteins derived from 7 human enteroviruses (representative of multiple species) and performed affinity purification followed by MS-analysis (AP-MS) of the co-purified endogenous human proteins (Supplementary Fig. 14). In this unbiased approach, SETD3 ranked amongst the top of the proteins (median MiST score = 0.98) alongside known 2A interacting proteins such as such as NUP98 (median MiST score = 0.99) and EIF4G1 (median MiST score = 0.86) (Supplementary Table 5, Fig. 4c, upper panel). Quantitative, targeted MS analysis showed that all tested enterovirus 2A proteins have a strong interaction with SETD3 compared to the mock control (Fig. 4c, lower panel). SETD3 was not significantly recovered in pull-downs with the unrelated 2A protein of EMCV or in additional negative controls including HIV Vif and EGFP, underscoring the specificity of the MS pull-downs (Supplementary Table 5). To further validate the 2A-SETD3 interaction in an orthogonal experimental system, we used the CheckMate mammalian two-hybrid system that detects protein-protein interactions in living cells (Supplementary Fig. 15a). Consistent with the AP-MS results, we found a strong activation of the reporter when both SETD3 and CV-B3 2A were co-expressed in cells, indicating that these proteins interact with each other. No substantial activation of the reporter was observed when both SETD3 and EMCV 2A were co-transfected into cells (Supplementary Fig. 15b). To identify specific CV-B3 2A residues that mediate the observed interaction with SETD3, we generated a library of CV-B3 2A mutants with systematic triplet-alanine substitutions spanning the entire protein. Using the same mammalian two-hybrid assay, we identified several 2A mutants (indicated in red) that abrogated the interaction with SETD3 (Fig. 4d). Western blotting analysis confirmed expression of all the 2A mutants except the 2A$^{(1-3)A}$ mutant (which was not detected) (Supplementary Fig. 16). When the residues identified by this analysis were mapped onto the coxsackievirus B 2A structure (PDB ID: 1Z8R) they clustered on a facet of 2A opposite to the catalytic triad (H18, D36, and C107) and around a highly conserved motif of cysteines (C55, C53, and C113) and a conserved histidine (H115) that coordinates zinc ion binding[24]. Although the function of the latter motif is unknown, disruption leads to loss of proteolytic activity[25]. To test whether proteolytic cleavage of 2A still occurs in SETD3^{KO} cells, WT and SETD3^{KO} cells were transfected with a construct expressing GFP fused to the C-terminal fraction of VP1 followed by catalytically active 2A (GFP-VP1-2A^{WT}). We found no apparent defect in *cis* (VP1-2A junction) or *trans* (EIF4G1) cleavage in the SETD3^{KO} cells (Supplementary Fig. 17). Interestingly, although direct mutation of the highly conserved motif (C53, C55, C113, and H115) was previously shown to disrupt catalytic activity[25], we found that SETD3-binding mutants, which harbor

mutations proximal to the conserved motif, largely retained catalytic activity. In particular, the *cis* and *trans*-cleaving activity of the $2A^{(136\text{-}138)A}$ mutant was indistinguishable from $2A^{WT}$ while other mutants were only mildly affected in their cleavage activity (Supplementary Fig. 18). Importantly, when these 2A mutations were introduced to the genome of full-length CV-B3-RLuc, there was a complete loss of RNA replication, suggesting that the interaction between 2A and SETD3 is critical for viral replication (Fig. 4e). Together, these data functionally link the 2A-SETD3 interaction to virus replication and uncover a previously unknown role of the enterovirus 2A in viral replication independent of protease activity.

Finally, we tested the contribution of SETD3 in infection of human primary cells and in *in vivo* mouse models of enterovirus pathogenesis. SETD3 was disrupted using CRISPR-Cas9 gene editing in primary normal human bronchial epithelial (NHBE) cells, a relevant primary cell type that is susceptible to multiple respiratory viruses including rhinoviruses A, B, and EV-D68 (Supplementary Fig. 19). When NHBE $SETD3^{KO}$ cells were infected with a panel of rhinoviruses and enterovirus D68 strains, a ~100-fold reduction in viral RNA accumulation was observed compared to wild-type NHBE cells (Fig. 5a). We then obtained mice heterozygous for the *Setd3* null allele from the Canadian Mouse Mutant Repository (Toronto, CA)[26]. Mice homozygous for the *Setd3* null allele ($Setd3^{-/-}$) were born without apparent developmental defects and were viable[12]. Intracerebral injection of neonates with CV-A10 and EV-A71[27] is a model for enterovirus pathogenesis resulting in systemic viral disease with high viral loads in the muscle, hind limb paralysis and ultimately death[28,29]. Indeed, in wild-type mice ($Setd3^{+/+}$) and heterozygous ($Setd3^{+/-}$) mice, we found that injection of CV-A10 and EV-A71 in 2-day-old pups resulted in hind-limb paralysis and death in the large majority of injected mice (Fig. 5b, 5c). In contrast, all $Setd3^{-/-}$ mice survived these lethal challenges and showed no symptoms of infection (Fig. 5b, 5c). This corresponded with a severe reduction in viral RNA accumulation in $Setd3^{-/-}$ mice at either 4 days (EV-A71) or 6 days (CV-A10) after infection, time points at which $Setd3^{+/+}$ and $Setd3^{+/-}$ mice show high viral loads in muscle tissue and brain (Fig. 5d, 5e, and Supplementary Fig. 20a, 20b). Intramuscular injection of EV-D68 MO resulted in mild symptoms in wild-type mice but viral RNA accumulation was readily detected at 6 dpi. In stark contrast, EV-D68 RNA levels were barely detectable in $Setd3^{-/-}$ animals (Fig. 5f).

Discussion

Overall, this study identifies the atypical host methyltransferase SETD3 as pivotal for infection by a broad panel of enteroviruses in human cells and in small animal models for enterovirus pathogenesis. We present a genome-wide and proteome-wide dissection of enterovirus biology highlighted by a recently discovered rhinovirus (RV-C15), a recent 2014 outbreak strain of enterovirus D68 isolated in the United States, and a highly contagious myocarditis virus (CV-B3). SETD3 knockout cells display a severe defect in RNA amplification while viral entry and initial translation are undisturbed. This is mechanistically distinct from two other enterovirus host factors PLA2G16 and CSDE1, which have shown to be important for viral entry and IRES-mediated translation, respectively[10,11]. Our work supports a model in which SETD3 engages the viral protein 2A protease via distinct domains to promote viral RNA replication in the cytoplasm. Interestingly, wild-type 2A

retained proteolytic activity in SETD3-knockout cells and SETD3-binding mutants of 2A imposed a strong replication defect while still being proteolytically active. This indicates that SETD3 is not strictly required for the protease activity of 2A although we cannot exclude that SETD3 more subtly influences the 2A proteolytic activity during viral infection. It has been proposed that 2A is a multifunctional protein with roles in translation[30] and RNA replication[31] independent of its proteolytic activity and SETD3 might promote such functions. The cardiovirus EMCV genome lacks a viral protein homologous to the enterovirus 2A protein and does not depend on SETD3 for cytopathic cell death emphasizing the specificity of the enterovirus 2A-SETD3 interaction[32,33].

Contrary to our expectations, our mechanistic studies revealed that the catalytic activity of neither viral protein 2A nor host protein SETD3 was necessary for the proviral effect of their binding interaction. Specifically, SETD3 was not required for 2A protease activity and inactivating the methyltransferase activity of SETD3 did not destroy the proviral effect. Instead, alanine scanning revealed a continuous surface on viral protein 2A, distinct from the active site, that is required for binding to SETD3 and viral growth. Recently, non-catalytic functions have been described for other SET-domain containing methyltransferases[34] and our results suggest that enteroviruses co-opted SETD3 by exploiting a non-catalytic function. Thus, the finding that a methyltransferase acts as a pro-viral host factor for the pathogenesis of a large class of viruses provides an interesting insight into how viruses must engage particular methyltransferases for viral replication and spread, while also being limited by related methyltransferases that promote antiviral immunity[15,16]. This emphasizes a largely unexplored and underappreciated role of host methyltransferases in viral pathogenesis. Notably, SETD3-null mice are viable and resistant to viral infection, suggesting that SETD3 is not essential for survival and development of the host. Therefore, SETD3 may serve as an attractive host-directed antiviral target to combat a broad range of medically important enteroviruses. Although small molecules targeting the catalytic activity of SETD3 would not necessarily act antiviral, our data provides rationale for the development of peptides or small molecule inhibitors that specifically block the SETD3-2A association and for the development of small molecules inducing SETD3 protein degradation using proteolysis-targeting chimaeras (PROTACs)[35].

Methods

Cells and reagents

C6/36 cells (CRL-1660), H1-Hela (CRL-1958), HEK293T (CRL-3216), and RD (CCL-136) cells were obtained from American Type Culture Collection (ATCC). 293FT cells (R70007) were purchased from Thermo Fisher. All transformed cell lines were cultured in DMEM/high glucose supplemented with 1× penicillin-streptomycin, 1× L-glutamine, and 10% heat-inactivated fetal bovine serum. Human primary normal bronchial epithelial cells (NHBE, Lonza CC-2540) were purchased from Lonza and cultured according to the manufacturer's recommendation using BEGM BulletKit (Lonza CC-3171 & CC-4175).

Viruses, reporter viruses, and infectious clones

Chikungunya virus (CHIKV, 18½5 vaccine strain) was a generous gift from Dr. Margaret Kielian and was propagated and titered by plaque assay on BHK-21 cells. Coxsackievirus A10 (CV-A10, Kowalik strain) was obtained from ATCC and was propagated and titered by plaque assay on RD cells. Coxsackievirus B3 Nancy strain that encodes Renilla luciferase (CV-B3-RLuc) was a generous gift from Dr. Frank van Kuppeveld, and was propagated by transfection of the infectious clone pRLuc-53CB3/T7 into RD cells, as described previously[36]. The titer of CV-B3-RLuc was determined by plaque assay on RD cells. Enterovirus A71 (EV-A71, MP4 infectious clone) was a kind gift from Dr. Jen-Ren Wang, and was propagated and titered as previously reported[29]. Enterovirus D68 (EV-D68) F02-3607-Corn strain (VR-1197) was obtained from ATCC. EV-D68 2014 outbreak isolates, i.e. Illinois isolate (US/IL/14-18952, NR-49131), Kentucky isolate (EV-D68 US/KY/14-18953, NR-49132), and Missouri isolate (EV-D68 US/MO/14-18947, NR-49129), were provided by BEI resources (NIH, NIAID). EV-D68 was propagated and titered by plaque assay on RD cells. Encephalomyocarditis virus (EMCV) Mengovirus strain vMwt (VR-1598) was purchased from ATCC and was propagated and titered by plaque assay on H1-HeLa cells. Poliovirus 1 (PV-1) Mahoney strain was a gift from Dr. Hidde Ploegh and propagated as well as titered on H1-HeLa cells. Rhinoviruses (RVs) A2 (RV-A2, VR-482) and B14 (RV-B14, VR-284) were obtained from ATCC. RVs were propagated and titered by plaque assay on H1-HeLa cells. Rhinovirus C15 (RV-C15) infectious clone (pC15-Rz)[37] was kindly provided by Drs. Ann Palmenberg and Yury Bochkov. To propagate RV-C15 virions, pC15-Rz was first linearized by *Bst*BI restriction digestion (New England Biolabs) and precipitated by 0.1 volume 3M sodium acetate, 0.05 volume 0.5M EDTA, and 2.5 volume 100% ethanol. The linearized plasmid was then in vitro transcribed using MEGAscript™ T7 Transcription Kit (Thermo Fisher). RV-C15 RNA was then transfected into H1-HeLa^{+CDHR3} cells using Lipofectamine 3000 (Thermo Fisher) to generate infectious RV-C15 virions. At 6 days post-transfection, RV-C15 virions were harvested from supernatant and cell lysates. The virions were used to further infect H1-HeLa^{+CDHR3} cells to produce higher titer RV-C15. The titer of RV-C15 was determined by plaque assay on H1-HeLa^{+CDHR3} cells. Recombinant vesicular stomatitis virus pseudotyped with glycoprotein of Ebola virus Zaire strain (rVSV-ZEBOV-GP GFP) was a gift from Dr. Sean Whelan and was propagated and titered by plaque assay on BHK-21 cells. Vesicular stomatitis virus (encoding GFP) is a gift from Dr. Jack Rose and was propagated on BHK-21 cells and titered using MA104 cells. An outbreak strain of Zika virus (ZIKV), PRVABC59 (Human/2015/Puerto Rico, NR-50240), was obtained from BEI resources (NIH, NIAID). ZIKV was propagated using C6/36 cells and titered by plaque assay on Huh7.5.1 cells.

Lentiviral packaging

Lentiviral transduction was performed on designated cell lines to generate cell lines that stably express proteins of interest. Respective constructs to express proteins of interest (see *Engineering of lentiviral constructs* section) were cloned by Gibson Assembly (New England Biolabs) into either the third generation lentiviral Gateway destination vector, pLenti-CMV-Puro-Dest (w118-1) (a gift from Eric Campeau), or pLenti-CMVTRE3G-Puro-DEST (w811-1) (Addgene, Plasmid #27565). Both plasmids harbor puromycin resistant gene as a marker for antibiotic selection. pLenti-CMV-Puro-Dest (w118-1) harbored the

high-expressing promoter, and pLenti-CMVTRE3G-Puro-DEST (w811-1) contained an inducible expression promoter that served as a low-expression promoter without the inducible transactivator present. Lentivirus was produced by co-transfection of the transgene expressing plasmid with a mixture of ΔVPR, VSV-G, and pAdVAntage packaging plasmids into 293FT cells using FuGENE HD (Promega). At 48 hours post-transfection, lentivirus was harvested from the supernatant and filtered through a 0.45-micron filter. 1× protamine sulfate was added to the lentivirus before transducing respective cell lines for overnight. H1-HeLa and H1-HeLa-derived cells that stably expressing the protein of interest were selected by treatment with 3 μg/ml of puromycin (InvivoGen) along with untransduced cells as negative controls.

Genome-scale CRISPR-Cas9 knockout screens

H1-HeLa cells were stably transduced with lentiCas9-Blast (Addgene, Plasmid #52962) and subsequently selected using blasticidin to generate constitutively expressing Cas9 H1-HeLa cells. A single Cas9-expressing H1-HeLa clone was then transduced with lentivirus without a selection marker to stably express CDHR3 C529Y (H1-HeLa^{+CDHR3}). A single H1-HeLa $^{+CDHR3}$ clone was then chosen based on RT-qPCR of CHDR3 expression and RV-C15 RNA levels for mutagenesis. A total number of 300 million H1-HeLa^{+CDHR3} cells constitutively expressing Cas9 were transduced with the lentiGuide-Puro from the GeCKO v2 library[38] at a MOI of 0.3. Cells were selected using puromycin and heterogeneous H1-Hela^{+CDHR3} knockout cell populations were subsequently pooled together. The CRISPR genetic screens were started 10 days post transduction. >1000-fold coverage of mutagenized cells (libraries A and B) was infected with either RV-C15 (MOI=1 PFU/cell) or EV-D68 Missouri (MOI=1 PFU/cell). RV-C15 infection was repeated for an additional round at 6 days post-infection. As soon as appearance of visibly viable colonies was observed, populations of virus-resistant cells were pooled and harvested. Uninfected starting populations of mutagenized cells were used as the unselected reference. Total genomic DNA from both virus-resistant and uninfected cells was respectively extracted using QIAamp DNA Mini Kit (Qiagen). The inserted guide RNA sequences were retrieved from the genomic DNA by PCR amplification. The PCR products were then purified and subjected to NextSeq platform (Illumina) next-generation sequencing. The sequencing data were processed and analyzed using MAGeCK algorithm[8] (version 0.5.4) to determine the ranking of each hit by taking the following criteria into account: the number of sequencing reads for each unique guide, the number of unique guide RNA per gene (i.e. 0-6), and the enrichment of a particular guide RNA in comparison to uninfected cell populations.

Generation of isogenic CRISPR-Cas9 knockout cell lines

H1-HeLa^{+CDHR3} SETD3^{KO} cell line was engineered using CRISPR-Cas9 strategy as previously described[39]. In brief, CRISPR guide RNA sequences were designed using the Zhang lab CRISPR design tool (http://crispr.mit.edu) and corresponding oligos were purchased from Integrated DNA Technologies. The oligos 5'-CACCGTGTTACAGAATGCAGCAGTC −3' and 5'-AAACGACTGCTGCATTCTGTAACAC −3' were cloned into the Cas9 expressing pX458 guide RNA plasmid (Addgene Plasmid #48138) using the target sequence cloning protocol provided by Feng Zhang group (http://www.genome-engineering.org/crispr). The cloning

products were transfected into H1-HeLa^{+CDHR3} cells using Lipofectamine 3000 (Thermo Fisher) according the manufacturer's guidelines. At 48 hours post-transfection, the cells were single-cell sorted based on GFP into 96-well plates using a BD Influx cell sorter at the Stanford Shared FACS facility. Clonal cell lines were allowed to expand from a single cell and genomic DNA was isolated for sequenced-based genotyping of targeted allele. For this, a ~500 base-pair (bp) region that encompassed the gRNA-targeted site was amplified and the sequence of the PCR product was determined by Sanger sequencing. Subclones were chosen in which all alleles were indels with insertions or deletions that were not a factor of 3. Oligo primers to perform the genotyping were 5'- AGCTAGGTGCTTGCTCAGTG −3' and 5'- GCCCCAGTACAAGACCTTTCA −3'. SETD3^{KO} subclones verified by genotyping were subsequently confirmed by western blot.

Engineering of SETD3 knockout human primary NHBE cells

To generate SETD3^{KO} human primary NHBE cells, the same CRISPR guide RNA was cloned into pLentiCRISPRV2 plasmid (Addgene, Plasmid #52961) as previously described[38]. The cloning product was transfected together with ΔVPR, VSV-G, and pAdVAntage packaging plasmids using FuGENE HD (Promega) to produce lentivirus in 293FT cells. In parallel, an empty pLentiCRISPRV2 plasmid was used to package lentivirus that served as a control. At 24 hours post-transfection, 293FT growth media was aspirated and replaced with NHBE growth media. At 48 hours post-transfection, lentivirus was harvested from the supernatant and filtered through a 0.45-micron filter. 1× protamine sulfate was added to the lentivirus before subjecting to transduce NHBE cells for 24 hours. At 48 hours post-transduction, 1ug/ml of puromycin was introduced to select for a population of SETD3^{KO} NHBE cells. The absence of SETD3 protein in the population of SETD3-deficient NHBE cells was confirmed by western blotting analysis.

Engineering of lentiviral constructs

To generate a lentiviral construct expressing CDHR3, human CDHR3 cDNA was purchased from Dharmacon (clone ID: 40037942). C529Y point mutation was introduced with primers 5'- GTAACTAAAGTGGACTATGAAACAACCCCCATC −3' and 5'- GATGGGGGTTGTTTCATAGTCCACTTTAGTTAC −3'. Amplified PCR product using primers 5'- TGTGGTGGAATTCTGCAGATACCATGCAGGAAGCAATCATTCTC −3' and 5'- CGGCCGCCACTGTGCTGGATTTACTTTCCTGGGTGTGGT −3' was then inserted into the EcoRV-digested pLenti-CMV-Puro-Dest (w118-1) by Gibson Assembly (New England Biolabs). To remove the puromycin resistance gene, pLenti-CMV-Puro-CHDR3 C529Y was digested with SpeI and XhoI (New England BioLabs). DNA Polymerase I, Large (Klenow) Fragment (New England BioLabs) was then used to generate blunt ends for T4 DNA ligation (New England BioLabs).

To generate a lentiviral construct expressing SETD3, SETD3 cDNA was purchased from OriGene (catalog #RC214566). SETD3 was PCR amplified using primers 5'- CACCATGGGTAAGAAGAGTCGAGTAAAAACTC −3' and 5'- CTACTCCTTAACTCCAGCAGTGC −3'. Amplified PCR product was then topo cloned into Gateway compatible entry vector pENTR™/D-TOPO® Cloning Kit (Life

Technologies), then inserted into pLenti-CMV-Puro-Dest(w118-1) by Gibson Assembly (New England Biolabs) using Gateway LR Clonase II (Thermo Fisher).

pgLAP6-SETD3 plasmid was provided by Dr. Peter Jackson. To generate a control lentiviral construct expressing GFP, GFP gene was PCR amplified from pgLAP6-SETD3 using primers 5'- TGTGGTGGAATTCTGCAGATACCATGGTGAGCAAGGGCG −3' and 5'-CTTGTACAGCTCGTCCATGC −3'. To add a C-terminal nuclear localization signal (NLS), GFP-SETD3 was amplified using forward primer 5'-GTGGTGGAATTCTGCAGATACCATGGTGAGCAAGGGCGAG −3' and reverse primers 5'-GCAGCAGGCTCCTTAACTCCAGCAGTGC −3' and 5'-GGCCGCCACTGTGCTGGATTTAGTCTAGTTTAACGCGTTTGGCAGCAGGCTCCTTAACTC −3'. To add a C-terminal nuclear export signal (NES), GFP-SETD3 was amplified using forward primer 5'- GTGGTGGAATTCTGCAGATACCATGGTGAGCAAGGGCGAG −3' and reverse primers 5'-GATCTACAGTTCCAGTTCTTCCAGCTTCTTCTGCAGCTCCTTAACTCCAGCAGTGCTG −3' and 5'- GGCCGCCACTGTGCTGGATCTACAGTTCCAGTTCTTCCAGC −3'. Amplified PCR products were then inserted into the EcoRV-digested doxycycline inducible lentiviral vector pLenti-CMVTRE3G-Puro-DEST (w811-1) by Gibson Assembly (New England BioLabs).

To generate lentiviral constructs expressing SETD4 and SETD6, cDNA sequences corresponding to the aforementioned Uniprot accession numbers were used as template for subcloning. SETD4 was PCR amplified with primers 5'-TGTGGTGGAATTCTGCAGATACCATGCAGAAAGGAAAAGGGAGAACAAG −3' and 5'- CGGCCGCCACTGTGCTGGATTCAGGTAAAAGCTGTTTGCAAACTGTG −3'. SETD6 was PCR amplified with primers 5'-TGTGGTGGAATTCTGCAGATACCATGGCGACCCAGGCGAAG −3' and 5'-CGGCCGCCACTGTGCTGGATCTAACTTGTCAGCTCCAACAACTGATG −3'. Amplified PCR products were then inserted into the EcoRV-digested pLenti-CMV-Puro-Dest(w118-1) by Gibson Assembly (New England BioLabs).

To generate lentiviral constructs expressing GFP-fusion SETD4, SETD6, SETD3$^{1-453}$, and SETD3$^{1-492}$ proteins, the N-terminal LAP6 tag was PCR amplified from pgLAP6 SETD3 using forward primer 5' – GTGGTGGAATTCTGCAGATACCATGGTGAGCAAGGGCGAGG – 3' and reverse primer 5' – GAAGCCTGCTTTTTTGTACAAACTTGTTTGATGAC – 3'. SETD4 was PCR amplified using forward primer 5' – GTACAAAAAAGCAGGCTTCATGCAGAAAGGAAAAGGGAGAACAAG – 3' and reverse primer 5' – CGGCCGCCACTGTGCTGGATTCAGGTAAAAGCTGTTTGCAAACTGTG – 3'. SETD6 was PCR amplified using forward primer 5' – GTACAAAAAAGCAGGCTTCATGGCGACCCAGGCGAAG – 3' and reverse primer 5' – CGGCCGCCACTGTGCTGGATCTAACTTGTCAGCTCCAACAACTGATG – 3'. SETD3$^{1-453}$ and SETD3$^{1-492}$ were PCR amplified as described for expressing C-terminal truncation mutants (see below). Amplified PCR products were then cloned into the EcoRV-digested pLenti-CMV-Puro-Dest(w118-1) by Gibson Assembly (New England BioLabs).

To generate lentiviral constructs expressing the SETD3–5M (W274A/N278A/H279A/Y313A/R316M) mutant, SETD3 Y313A construct[12] was used a template to sequentially incorporate W274A and R316M mutations by Phusion site-directed mutagenesis using the following primer pairs: (W274A) 5’ – GCGGATATGTGTAACCAC – 3’, 5’ – TAAAGGAATCAGAGC, and (R316A) 5’ – GCATCCAACGCAGAGTTTG– 3’, 5’ – AGTGCCAGCAAAAATG– 3’. The final point mutations (N278A/H279A) were introduced to SETD3 by PCR using the following primer pair: 5’ – CTTTAGCGGATATGTGTGCCGCCACCAACG – 3’ and 5’ – CGTTGGTGGCGGCACACATATCCGCTAAAG – 3’. This SETD3-5M mutant was introduced to either EcoRV-digested pLenti-CMV-Puro-Dest(w118-1) or EcoRV-digested pLenti-CMVTRE3G-Puro-DEST(w811-1) by Gibson Assembly (New England BioLabs).

To generate lentiviral constructs expressing a series of C-terminal truncation mutants for SETD3, the following primer pairs were used to PCR amplify inserts that were subsequently cloned into the EcoRV digested pLenti-CMV-Puro-Dest (w118-1) by Gibson Assembly (New England Biolabs). The forward primer was 5’-TGTGGTGGAATTCTGCAGATACCATGGGTAAGAAGAGTCGAGTAAAAACTCAG −3’ and used with the following reverse primers:

$SETD3^{1\text{-}594}$ (full length)

5’- CGGCCGCCACTGTGCTGGATCTACTCCTTAACTCCAGCAGTGC −3’

$SETD3^{1\text{-}327}$

5’- CGGCCGCCACTGTGCTGGATCTAAAAACCACTGTGGATCACAAACTC −3’

$SETD3^{1\text{-}344}$

5’- CGGCCGCCACTGTGCTGGATCTAACTCACTCCAAGCTTTATTTTCACTCTG −3’

$SETD3^{1\text{-}373}$

5’- CGGCCGCCACTGTGCTGGATCTAGGTAAAATGCAATGCAAAAACACTGG −3’

$SETD3^{1\text{-}401}$

5’- CGGCCGCCACTGTGCTGGATCTATCCCAGCAAGTGTTCTTTCAG −3’

$SETD3^{1\text{-}453}$

5’-CGGCCGCCACTGTGCTGGATCTATTTCAAGACGGATTTATCTTCCTCAATAGTTG −3’

$SETD3^{1\text{-}492}$

5’- CGGCCGCCACTGTGCTGGATCTACTGTTGGCGATAGTATTCCCGG −3’

$SETD3^{1\text{-}527}$

5’- CGGCCGCCACTGTGCTGGATCTACTCGAGGTTTCTCAAGACCAGG −3’

SETD3$^{1\text{-}563}$

5’- CGGCCGCCACTGTGCTGGATCTAGGTCCCATTAGGGATAGAGTTTTCAC −3’

To generate lentiviral constructs expressing SETD3 with a C-terminal FLAG tag, the following primers were used to create an in-frame fusion: 5’ – TGTGGTGGAATTCTGCAGATACCATGGGTAAGAAGAGTCGAGTAAAAACTCAG – 3’ , 5’ – CGTCGTCATCCTTGTAATCCTCCTTAACTCCAGCAGTGC – 3’, and 5’ – CGGCCGCCACTGTGCTGGATCTACTTATCGTCGTCATCCTTGTAATCCTCC – 3’. To generate lentiviral constructs expressing the GFP-Rubisco Substrate Binding Domain (SETD3 328-594)-FLAG, SETD3-FLAG was used as a template for PCR amplification using 5’ – GCATGGACGAGCTGTACAAGATGTTCTTTGACAATAACTCACACGACAGAG – 3’ and 5’ – GTGAGTTATTGTCAAAGAACATCTTGTACAGCTCGTCCATGC – 3’. The PCR amplicon for GFP was described above. All PCR amplicons were cloned into the EcoRV-digested pLenti-CMV-Puro-Dest(w118-1) by Gibson Assembly (New England BioLabs).

Quantitation of virus infectivity by quantitative RT-PCR (qRT-PCR)

Cells were seeded on 96-well plates (Greiner Bio-One) and incubated overnight before being infected by designated viruses with the indicated multiplicity of infection (MOI). At designated time points, cell lysates were harvested using the Ambion Cells-to-CT kit (Thermo Fisher) according the manufacturer’s protocol. After reverse transcription (RT) reaction, quantitative PCR (qPCR) was performed. Viral RNA levels were normalized to 18S RNA levels.

The following primers (5’−3’ orientation) were used for the qPCR:

18S-Fwd: AGAAACGGCTACCACATCCA

18S-Rev: CACCAGACTTGCCCTCCA

CV-A10-Fwd: CACTCAACCGGTTTTGGATT

CV-A10-Rev: TAGTTGTGCCACTCGGTCAC

EV-A71-Fwd[40]: CCCTGAATGCGGCTAATCC

EV-A71-Rev[40]: ATTGTCACCATAAGCAGCCA

EV-D68-Fwd[41]: GGTGTGAAGAGTCTATTGAGC

EV-D68-Rev[41]: CACCCAAAGTAGTCGG

RV-A2-Fwd: ACCTGGCAGATGAGGCTAGA

RV-A2-Rev: TGTTTGGCTTCACACCCATA

RV-B14-Fwd: AGTTGGCCCTGTAACAATGG

RV-B14-Rev: TGCCCAGTTTTTGTTGCATA

RV-C15- Fwd: AATTCTCAGGTGCCATGGAG

RV-C15- Rev: GTTGGGTGATTGCTCATCCT

Note that the downward error bar in Figure 1d, panel d (SETD3^{KO}, 48 hpi) was omitted because it would reach a negative value that is invalid on a logarithmic scale.

Crystal violet staining

H1-HeLa^{+CDHR3} (WT) cells, SETD3^{KO} cells, and SETD3^{KO} cells complemented with SETD3 were seeded onto 24-well or 96-well plates (Greiner Bio-One). Cells were subsequently infected with RV-A2 (MOI=1), RV-B14 (MOI=1), RV-C15 (MOI=25), EV-D68 F02-3607-Corn (MOI=0.5), EV-D68 Illinois (MOI=10), EV-D68 Missouri (MOI=100), EV-D68 Kentucky (MOI=5), CV-A10 (MOI=1), CV-B3 (MOI=1), PV-1 Mahoney (MOI=1), Mengo virus (MOI=0.1), CHIKV (MOI=1), rVSV-Ebov (MOI=1), ZIKV PRVABC59 (MOI=25). Cells were incubated at either 34°C (for all RV and EV-D68) or 37°C (other viruses) for 24 to 96 hours before being fixed using 4% formaldehyde in PBS. Cell viability at time of fixation was determined by standard crystal violet staining.

RV-B14 luciferase replicon assays

RV-B14 replicon (pΔP1Luc/VP3)[42] was a generous gift from Dr. Frank van Kuppeveld. RV-B14 replicon RNA was first linearized by *SmaI* (New England Biolabs) restriction digestion and then precipitated by 0.1 volume 3M sodium acetate, 0.05 volume 0.5M EDTA, and 2.5 volume 100% ethanol. Next, the linearized plasmid was in vitro transcribed using MEGAscript™ T7 Transcription Kit (Thermo Fisher). Cells were washed twice with 1×phosphate buffered saline (HyClone) and re-suspended in electroporation buffer (Teknova E0399). 3 μg of the replicon RNA was were electroporated into 2 million cells using square wave protocol (Bio-Rad Gene Pulser Xcell electroporator). Electroporated cells were resuspended in H1-HeLa culture medium without antibiotics and seeded into 6-well plates. At 24 hours post-electroporation, total cell lysates were harvested in passive lysis buffer and luciferase expression was measured using Luciferase Assay System (Promega E1500). Luciferase activity was measured by addition of substrate and readings were taken immediately using Glomax 20/20 luminometer using a 5 second integration time. In parallel, 3 μg Firefly luciferase mRNA (capped, Trilink) was electroporated into the same set of cells as a control to test if the loss of SETD3 could have universal impact on cap-dependent translations.

Luciferase reporter virus (CV-B3-RLuc) synchronized infection assays

Cells were seeded on 96-well plates (Greiner Bio-One) in triplicates and incubated for 16 to 24 hours. Cells were first pre-chilled on ice for 30 minutes. Next, CV-B3-RLuc (MOI=10) were pre-bound to cells on ice for 60 minutes in the presence of either dimethyl sulfoxide (DMSO, Thermo Fisher) at a final concentration of 0.1%, guanidine hydrochloride (GuHCl, Sigma-Aldrich) at a final concentration of 2 mM or cycloheximide (CHX, Sigma-Aldrich),

at a final concentration of 125 μM. The cells were then incubated at 37°C in incubator for 10 minutes to permit viral entry. Next, the cells were washed 3 times with PBS and cultured in complete culture media supplemented with DMSO, GHCl, or CHX at the above-mentioned final concentration. At indicated time points, total cell lysates were harvested in Renilla Luciferase Assay lysis buffer and luciferase expression was measured using Renilla Luciferase Assay system (Promega E2820). Luciferase activity was measured by addition of substrate and luciferase readings were taken immediately using Glomax 20/20 luminometer using a 5 second integration time.

Immunofluorescence

Indicated H1-HeLa cells were seeded overnight onto autoclaved 12mm circle micro cover glass (VWR) at 50,000 cells per well in 24-well plates (Greiner Bio-One). For studies involving CV-B3 infection, cells were infected with CV-B3 at MOI=5 for the indicated timepoints. Samples were fixed with 4% paraformaldehyde (Sigma) for 30 minutes at room temperature. Anti-GFP (Invitrogen, A-11122, 1:300) in immunofluorescence blocking buffer (1× phosphate buffered saline (PBS) with 3% BSA, 1% saponin and 1% Triton X-100) was incubated with each sample overnight at 4°C. Cells were washed five times in 1×PBS (Hyclone) before being incubated for 1 hour at room temperature with Alexa488 anti-rabbit antibody (1:500) (Life Technologies, A-11008, 1:500) and DAPI stain (1:300) (Insitus Biotechnologies, NC0407502, 1:300) in immunofluorescence blocking buffer. Samples were washed a final five times in 1×PBS (Hyclone). Micro cover glasses were then mounted onto microscope slides (Thermo Fisher) using Vectashield with DAPI (Vector Laboratories Inc). Images were taken with Zeiss LSM 700 confocal microscope and processed with Velocity software.

RNA Sequencing

Total RNA from WT and SETD3^{KO} H1-Hela^{+CDHR3} cells in duplicate was extracted using TRIzol Reagent (Ambion) according to manufacturer's guidelines. RNA sample quality was measured by both NanoDrop spectrophotometer (Thermo Fisher) and Bioanalyzer 2100 (Agilent). Libraries were sequenced on the BGISEQ-500 platform and the SE reads were aligned to the GRCh37 (hg19) genome assembly using Bowtie2 to map clean reads to reference gene and using HISAT2 to reference genome with the following parameters: --phred64 --sensitive -I 1 -X 1000. FPKM (Fragments Per Kilobase Million) reads were counted using Subread and differential gene expression analysis was performed using DESeq2BGI differential gene expression analysis was performed using DESeq2BGI based on the non-parametric Noiseq method.

Quantitative RT-PCR analysis for innate immune responses

Wild-type and SETD3 knockout cells were stimulated with recombinant human IFN-β (100 U/ml) for 8 or 24 hr, or infected with indicated viruses (MOI=5) for 8 hr. Total RNA was harvested into RLT buffer supplemented with β-mercaptoethanol (1:100) and extracted using RNeasy Mini kit (Qiagen) as previously described[43]. Random hexamer was used for reverse transcription reaction using 1 μg of RNA and High-Capacity cDNA Reverse Transcription Kit (Thermo Fisher). QPCR was performed with the Stratagene Mx3005P (Agilent) with a

25 μl reaction consisting of 5 μl of cDNA, 12.5 μl of Power SYBR Green master mix (Applied Biosystems), and 200 nM both forward and reverse primers.

IFN-β (RefSeq NM_002176):

Forward: ATGACCAACAAGTGTCTCCTCC,

Reverse: GGAATCCAAGCAAGTTGTAGCTC;

IFN-λ3 (RefSeq NM_172139):

Forward: TAAGAGGGCCAAAGATGCCTT,

Reverse: CTGGTCCAAGACATCCCCC;

MX1 (RefSeq NM_001144925):

Forward: GTGGCTGAGAACAACCTGTG,

Reverse: GGCATCTGGTCACGATCCC;

CXCL10 (RefSeq NM_001565):

Forward: GTGGCATTCAAGGAGTACCTC;

Reverse: TGATGGCCTTCGATTCTGGATT;

GAPDH (RefSeq NM_002046):

Forward: GGAGCGAGATCCCTCCAAAAT,

Reverse: GGCTGTTGTCATACTTCTCATGG.

All SYBR Green primers have been validated with both dissociation curves and DNA electrophoresis of the correct amplicon size.

Phylogenetic Tree

The following protein sequences were retrieved from the NCBI protein database: EZHI (Q92800), EZH2 (Q15910), SETD2 (Q9BYW2), ASH1L (Q9NR48), NSD2 (O96028), NSD3 (Q9BZ95), KMT2A (Q03164), KMT2D (O14686), KMT2C (Q8NEZ4), KMT2B (Q9UMN6), SETD1A (O15047), SETD1B (Q9UPS6), KMT2E (Q8IZD2), SETD5 (Q9C0A6), SUV39H1 (O43463), SUV39H2 (Q9H5I1), SETDB1 (Q15047), SETDB2 (Q96T68), EHMT1 (Q9H9B1), EHMT2 (Q96KQ7), SETMAR (Q53H47), SMYD1 (Q8NB12), SMYD2 (Q9NRG4), SMYD3 (Q9H7B4), SMYD4 (Q8IYR2), SMYD5 (Q6GMV2), SETD3 (Q86TU7), SETD4 (Q9NVD3), SETD6 (Q8TBK2). The phylogenetic tree of the select SET domain family members was determined from the protein sequence alignments created using Clustal Omega (https://www.ebi.ac.uk/Tools/msa/clustalo/) and was constructed using ggtree (version 3.3.3) in R studio.

Targeted quantification of Actin H73 methylation by mass spectrometry

LC-MS/MS was performed using an Orbitrap Elite (Thermo Scientific) and data was analyzed manually or using MaxQuant software (version 1.5.5.1)[44]. Peptide identification searches with MaxQuant were performed with parameters to identify methionine oxidation, N-terminal acetylation, and methyl histidine. Targeted quantification of actin methylation was performed by manual identification of methylated and unmethylated peptides followed by integration of area under the curve for chromatographic peaks associated with the corresponding *m/z*. Percentage of methylated peptides was determined as a fraction of the sum total area for methylated and unmethylated species. Actin was isolated from indicated H1-Hela cell lines by DNAse I affinity chromatography[45]. DNAse I was immobilized to NHS-activated Sepharose FF (GE Healthcare) overnight in 100 mM Hepes pH 7.5, 150 mM NaCl, 80 mM $CaCl_2$. Cells were homogenized with buffer containing 1M Tris pH 8.0, 600 mM KCl, 0.5 mM $MgCl_2$, 4% NP-40, 1% Tween-20, 1 mM DTT, 1 mM ATP, and Complete protease inhibitors[46] (Roche). Cleared lysates in all cases were incubated with affinity media overnight, washed, boiled in SDS sample buffer, and purified protein was resolved by SDS-PAGE. Gels were silver-stained (Thermo Scientific) then band corresponding to actin was excised and processed for mass spectrometry by in-gel digest with sequencing grade trypsin (in 50 mM ammonium bicarbonate) or Glu-C (in phosphate buffer), respectively.

In vitro methylation reactions

SETD3 (Q86TU7), actin (ACTB, P60709), and CV-B3 $2A^{C107A}$ (GenBank: M33854.1) were cloned into pGEX-6P-1. Truncated SETD3 constructs were generated using Phusion Site-Directed mutagenesis (Thermo Scientific) according to manufacturer's recommendations. All proteins were expressed as N-terminal GST fusions in BL21 bacteria. Expression was performed at 20°C overnight in the presence of 0.1 mM IPTG. Recombinant proteins were purified with Glutathione sepharose 4B (GE Healthcare) and eluted with 10 mg/ml reduced glutathione (Sigma-Aldrich), 100 mM Tris pH 8.0, and 20% glycerol. *In vitro* methyltransferase reactions were performed with 5 μg SETD3, 1 μg substrate, and 2 μCi ^{3}H-*S*-adenosylmethionine in a buffer containing 50 mM Tris pH 8.0, 20 mM KCl, 5 mM $MgCl_2$ at 30°C overnight. Reactions were resolved by SDS-PAGE and ^{3}H-methylation was visualized by autoradiography and gels were stained with Coomassie.

CV-B3 viral gene expression constructs

Coxsackie virus B3 genes (Nancy strain, GenBank: M33854.1) were individually PCR-amplified from a genomic plasmid using primers containing restrictions site overhangs, digested, and ligated into the pcDNA4/TO plasmid (Invitrogen) that has been engineered to fuse a 2xStrep tag to the C-terminus of proteins cloned into the multiple cloning site[47]. Mutations for 2A C107A and 3C C147A were introduced by site-directed mutagenesis.

Affinity purification for CV-B3 proteins mass spectrometry

293T and Huh7 cells were transfected with plasmids using PolyJet reagent (Signagen). Cells were lysed 48 hours post-transfection in IP buffer with detergent (150mM NaCl, 50mM Tris pH 7.4, 1mM EDTA, 0.5% NP-40 substitute) for 30 min at 4°C. Clarified lysates were affinity-purified with Streptactin Superflow Resin (IBA, 2-1206-025) at 4°C overnight.

Resin was washed three times in IP buffer with detergent, followed by one wash in IP buffer without detergent (150mM NaCl, 50mM Tris pH 7.4, 1mM EDTA). Protein complexes were eluted in 40μl IP buffer without detergent containing 2mM biotin at room temperature for 10 minutes, with agitation. 10 μl of the eluate was subjected to mass spectrometry analysis and a portion of the remainder for analysis by SDS-PAGE followed by either western blotting or silver staining.

Sample preparation for CV-B3 proteins mass spectrometry

Purified protein eluates were digested with trypsin for LC-MS/MS analysis. Samples were first denatured and reduced in 2M urea, 10 mM NH4HCO3, 2 mM DTT for 30 min at 60°C, then alkylated with 2 mM iodoacetamide for 45 min at room temperature. Trypsin (Promega) was added at a 1:100 enzyme:substrate ratio and digested overnight at 37°C. Following digestion, samples were concentrated using C18 ZipTips (Millipore) according to the manufacturer's specifications. Desalted samples were evaporated to dryness and resuspended in 0.1% formic acid for mass spectrometry analysis.

CV-B3 proteins mass spectrometry

Digested peptide mixtures were analyzed by LC-MS/MS on a Thermo Scientific Velos Pro dual linear ion trap mass spectrometer. The Velos Pro system was equipped with a Proxeon Easy-nLC II HPLC with a pre-column (2 cm x 100 um I.D. packed with ReproSil Pur C18 AQ 5 um particles) and an analytical column (10 cm x 75 um I.D. packed with ReproSil Pur C18 AQ 3 um particles). A gradient was delivered from 5% to 30% ACN in 0.1% formic acid over one hour. Data was collected in data-dependent fashion, collecting one full scan followed by 20 collision-induced dissociation MS/MS scans of the 20 most intense peaks from the full scan. Dynamic exclusion was enabled for 30 seconds with a repeat count of 1. Data were searched using the Protein Prospector algorithm against a database containing SwissProt Human protein sequences and CV-B3 sequences, concatenated to a decoy database where each sequence was randomized in order to estimate the false positive rate[48]. The searches considered a precursor mass tolerance of 1 Da and fragment ion tolerances of 0.8 Da, and considered variable modifications for protein N-terminal acetylation, protein N-terminal acetylation and oxidation, glutamine to pyroglutamate conversion for peptide N-terminal glutamine residues, protein N-terminal methionine loss, protein N-terminal acetylation and methionine loss, and methionine oxidation, and constant modification for carbamidomethyl cysteine. Prospector data was filtered using a maximum protein expectation value of 0.01 and a maximum peptide expectation value of 0.05. The searched data was then scored for protein-protein interactions (PPIs) using the MiST algorithm[18], with spectral counts as the quantifying feature of the data. High-confidence PPIs was required a MiST score greater than or equal to 0.75.

Co-Immunoprecipitations

Human codon-optimized $2A^{C107A}$ protein sequences for CV-B3 (Nancy strain, GenBank: M33854.1) and EMCV (Ruckert strain[49]) were cloned into pcDNA/TO plasmid for expression with a C-terminal 2xStrep tag (see *CV-B3 viral gene expression constructs*). (Note: the same CV-B3 2A sequence was used for affinity mass spectrometry and mammalian two-hybrid analysis). An N-terminal FLAG-tag was fused in frame to the

SETD3, SETD3$^{1-453}$, or SETD3$^{1-492}$ coding sequence using the following PCR primers: 5' – CCATGGATTACAAGGATGACGACGATAAGATGGGTAAGAAGAGTCGAGTAAAAACTCAG – 3', 5' – TGTGGTGGAATTCTGCAGATACCATGGATTACAAGGATGACGACG – 3', and 5' – CGGCCGCCACTGTGCTGGATCTACTCCTTAACTCCAGCAGTGC – 3'. The FLAG-SETD3 PCR amplicon was then cloned into the EcoRV-digested pLenti CMV-Puro-Dest (w118-1) by Gibson Assembly (New England BioLabs). Transfections with FLAG-SETD3 and either CV-B3 2A-2xStrep or EMCV 2A-2xStrep were carried out with Lipofectamine 3000 (ThermoFisher Scientific) according to the manufacturer's instructions in HEK 293FT cells seeded the day before transfection into 24-well plates (Greiner Bio-One) at 200,000 cells per well. Co-immunoprecipitation protocol was previously described[39]. Briefly, at 48 hours post-transfection, cells were washed once with 1xPBS (Hyclone) before lysis with TNM buffer (25 mM Tris-HCl, 15mM NaCl, 5mM $MgCl_2$) containing 1% Halt Protease and Phosphatase Inhibitor Cocktail (Life Technologies) for 1 hour on ice gently vortexing every ~15 minutes. Cell lysates were centrifuged at 15,000 x *g* for 10 minutes, and clarified lysates were incubated overnight at 4°C with anti-FLAG M2 Magnetic Beads (Sigma) – 5% of clarified lysate was saved for input fraction. Incubated beads were washed 3X with TNM buffer containing protease inhibitor, then 2X with just TNM buffer before eluting with TNM buffer containing 150 ng/μl 3x FLAG peptide (Sigma) on ice for 30 minutes. Samples were prepared for western blotting analysis (see *Western blotting analysis*). Anti-SETD3 (Abcam, ab176582, 1:5000) and anti-Strep-HRP (IBA lifesciences, 2-1509-001, 1:10,000) were used for protein detection.

SETD3 tandem affinity purification and mass spectrometry

Tandem-affinity purification and mass spectrometry service was conducted by Dr. Peter Jackson's laboratory SNAP team and the Stanford University Mass Spectrometry Core. Briefly, SETD3 cDNA was cloned into pgLAP6 expression vector to generate a stable doxycycline-inducible LAP6-SETD3 expressing HEK 293 T-REx cell line. After 24-hour doxycycline induction of LAP6-SETD3, HEK 293 T-REx cells were then infected with coxsackievirus A10 (MOI=1 PFU/cell) and cell lysates were harvested 24 hpi. IP-MS analysis was carried out as previously described[23,43].

Affinity purification of Strep- and FLAG-tagged proteins.

HEK293T cells cultured in Dulbecco's Modified Eagle's medium (DMEM) supplemented with Fetal bovine serum and Pen-Strep were plated 20-24 hours prior to transfection. For each single-step purification, a single 14.5 cm dish was transfected with 15-20 μg plasmid using PolyJet Transfection Reagent (SignaGen Laboratories) at a 1:3 ratio of plasmid to transfection reagent. Affinity purifications were performed based on previous descriptions[50,51]. In brief, about 40 hours post-transfection cells were harvested and lysed in IP Buffer (50 mM Tris-HCl pH 7.4, 150 mM NaCl, 1 mM EDTA) supplemented with 0.5% Nonidet P 40 Substitute (NP40; Fluka Analytical), cOmplete mini EDTA-free protease and PhosSTOP phosphatase inhibitor cocktails (Roche) and incubated for 30 minutes. Cleared cell lysates were added to equilibrated with MagStrep "type 3" magnetic beads (IBA Lifesciences) or anti-FLAG M2 magnetic beads (Sigma) and incubated for 2 hours at 4°C. After binding, beads were washed three times with 1 ml IP Buffer supplemented with 0.05%

NP40 and once with detergent free IP Buffer. Bound proteins were subjected to on-bead digestion for mass spectrometry (described below) and 20% or the beads were kept for biotin elution and western blot analysis. Strep- and FLAG-tagged proteins were eluted with BXT Buffer containing 50 mM biotin (IBA Lifesciences) or 0.1 mg/ml 3xFLAG peptide in IP Buffer supplemented with 0.05% RapiGest, respectively at room temperature for 30 minutes. Lysates and 10% of eluates were resolved on 4-20% Criterion protein gels (Bio-Rad Laboratories) to assess Strep- and FLAG-tagged protein expression and purification by western blot and silver stain (ThermoFisher Scientific), respectively, before submitting 10 μl eluate for mass spectrometry. Three to four independent biological replicates were performed for FLAG and Strep purifications.

Mass spectrometry analysis and scoring for global single and double AP-MS experiments.

Peptides from single and double affinity purifications were analyzed on a Q-Exactive Plus (Thermo Fisher) mass spectrometer. The Q-Exactive Plus system was equipped with an Easy1200 nLC system (Thermo Fisher) and an analytical column (25 cm x 75 um I.D. packed with ReproSil Pur C18 1.9 μm, 120Å particles, Dr. Maisch). A gradient was delivered from 4.5% to 32% acetonitrile over 53 minutes at a flow rate of 300 nl/min. All MS spectra were collected with Orbitrap detection, while the 20 most abundant ions were fragmented by HCD and detected in the Orbitrap. Peptide and protein identification searches, as well as label-free quantitation were performed using the MaxQuant data analysis algorithm (version 1.5.2.8)[44]. Data were searched against a database containing SwissProt Human sequences (downloaded 07/2018) as well as enterovirus 2A protein sequences, concatenated to a decoy database where each sequence was randomized in order to estimate the false discovery rate (FDR).

Variable modifications were allowed for methionine oxidation and protein N-terminus acetylation. A fixed modification was indicated for cysteine carbamidomethylation. Full trypsin specificity was required. The first search was performed with a mass accuracy of +/− 20 parts per million (ppm) and the main search was performed with a mass accuracy of +/− 4.5 parts per million. A maximum of 5 modifications were allowed per peptide. A maximum of 2 missed cleavages were allowed. The maximum charge allowed was 7+. Individual peptide mass tolerances were allowed. For MS/MS matching, a mass tolerance of +/− 20 ppm was allowed and the top 12 peaks per 100 Da were analyzed. MS/MS matching was allowed for higher charge states, water and ammonia loss events. The data were filtered to obtain a peptide, protein, and site-level false discovery rate of 0.01. The minimum peptide length was 7 amino acids.

The Maxquant results from the single 2A affinity purifications were scored for specific protein-protein interactions (PPIs) using the MiST algorithm[18], with spectral counts as the quantifying feature of the data. Protein spectral counts for each sample were calculated as the sum from the peptide spectral counts for one protein in a given sample. High-confidence PPIs was required a MiST score greater than or equal to 0.75.

The Maxquant results from the single SETD3 affinity purifications were scored for specific protein-protein interactions (PPIs) using the SAINTexpress (Significance Analysis of INTeractome) algorithm[52,53], with spectral counts as the quantifying feature of the data.

HEK293T cells transfected with an empty vector (not expressing any affinity tagged bait) were used as control condition and were processed and analyzed in parallel with the bait protein expressing cells in order to avoid batch effects. Protein spectral counts for each sample were calculated as the sum from the peptide spectral counts for one protein in a given sample. To discriminate bona fide protein interactors of SETD3 in the presence and absence of CV-B3 2A for each infection condition from the control, we set a FDR threshold of 0.05. To generate an overall list of candidate interactors for SETD3, we combined the proteins with an FDR below 0.05 for both conditions (+/− CV-B3 2A expression).

Targeted mass spectrometric assay generation, data acquisition and analysis.

SRM assay generation was performed using Skyline[54]. For all targeted proteins, proteotypic peptides and optimal transitions for identification and quantification were selected based on a spectral library generated from the global AP-MS experiments. The Skyline spectral library was used to extract optimal coordinates for the SRM assays, e.g. peptide fragments and peptide retention times. For each protein 3-8 peptides were selected based on intensity, peptide length as well as chromatographic performance. For each peptide, the 3-5 best SRM transitions were selected based on intensity and peak shape.

Digested peptide mixtures were analyzed by LC-SRM on a Thermo Scientific TSQ Quantiva MS system equipped with a Proxeon Easy nLC 1200 ultra high-pressure liquid chromatography and autosampler system. Samples were injected onto a C18 column (25 cm x 75 um I.D. packed with ReproSil Pur C18 AQ 1.9um 120Å particles, Dr. Maisch) in 0.1% formic acid and then separated with an 53 min gradient from 7% to 36% Buffer B (80% ACN/20% water/0.1% formic acid) at a flow rate of 300 nl/min. SRM acquisition was performed operating Q1 and Q3 at 0.7 unit mass resolution. For each peptide, the best 3-5 transitions were monitored in a scheduled fashion with a retention time window of 5 min and a cycle time fixed to 2.5 sec. Argon was used as the collision gas at a nominal pressure of 1.5 mTorr. Collision energies were calculated by, $CE = 0.0348 * (m/z) + 0.4551$ and $CE = 0.0271 * (m/z) + 1.5910$ (CE, collision energy and m/z, mass to charge ratio) for doubly and triply charged precursor ions, respectively. SRM data was processed using Skyline. Protein significance analysis was performed using MSstats[55].

Mammalian two-hybrid assay for protein-protein interactions

pACT, pBIND, and pG5luc plasmids were obtained from the Checkmate Mammalian Two-hybrid System (Promega). 2A protein sequence for CV-B3 (Nancy strain) and EMCV (Ruckert strain) were codon-optimized for human expression (Note: the same CV-B3 2A sequence was used for *AP mass spectrometry* and *Co-immunoprecipitation*). SETD3 were PCR amplified and subsequently cloned into the EcoRV restriction site of pBIND by Gibson Assembly (New England BioLabs). $2A^{C107A}$ were PCR amplified and subsequently cloned into the EcoRV restriction sites of pACT by Gibson Assembly (New England BioLabs). The following primers were used (5'−3' orientation):

SETD3-Fwd:
CGTCGACTTGACGCGTTGATAATGGGTAAGAAGAGTCGAGTAAAAACTCAG

SETD3-Rev:

CTGCGGCCGCTCTAGATGATCTCCTTAACTCCAGCAGTGCTG

CV-B3-Fwd:

CGTCGACTTGACGCGTTGATAGGACAACAGTCTGGCGCAG

CV-B3-Rev:

CTGCGGCCGCTCTAGATGATCTGTTCCATCGCGTCGTCC

EMCV-Fwd:

CGTCGACTTGACGCGTTGATAAGTCCTAACGCCCTTGACATCAGC

EMCV-Rev:

CTGCGGCCGCTCTAGATGATCCCCGGGTTCGTTTCAATGTCG

To identify residues in CV-B3 2A important for interaction with SETD3, three consecutive residues in the CVB3 2A coding sequence were substituted to alanine per construct to generate 49 mutant proteins. Mutations in 2A were either introduced using QuikChange Lightning Multi Site-Directed Mutagenesis Kit (Agilent Technologies) or gene block synthesized (Integrated DNA Technologies). All DNA cloning products were validated by Sanger DNA sequencing. Analysis was performed with the pACT-2A and pBIND-SETD3 fusion pair because those plasmids generated the least background signal when expressed individually. HEK 293FT cells were seeded the day before transfection into 24-well plates (Greiner Bio-One) at 200,000 cells per well for interaction studies for Supplementary Figure 15, and into 96-well plates (Greiner Bio-One) at 50,000 cells per well for the alanine scanning. Transfections were performed with equal amount (1:1:1 ratio) of each plasmids (bait, prey, and reporter plasmid) using Lipofectamine 3000 (Thermo Fisher Scientific) according to the manufacturer's instructions. Negative controls included transfections with empty pACT and empty pBIND, pACT-2A and empty pBIND, and empty pACT and pBIND-SETD3 were included. Renilla and Firefly luciferase signal was measured with the Dual Luciferase Reporter Assay System (Promega) at 48 hours post-transfection according to the manufacturer's protocol using a Glomax 20/20 luminometer with a 5 second integration time. Measurements were normalized to Renilla luciferase production generated from the pBIND or pBIND-SETD3 plasmid. Expression of the protein fusion constructs at 48 hours post-transfection was confirmed by western Blot analysis (see *Western blotting analysis*) using anti-VP16 (Santa Cruz, sc-7546, 1:500) and anti-GAL4 (Santa Cruz, sc-510, 1:500). Anti-P-84 (Genetex, GTX70220, 1:5000) was used as a loading control.

Visualization of coxsackievirus 2A 3-dimensional structure

We used 2A protease crystal structure from human coxsackievirus B4 (strain JVB/ Benschoten /New York/51) (PDB: 1Z8R), which is closely related to CV-B3, as a template to visualize various functional motifs of CV-B3 2A. Molecular graphics and analyses on the CV-B4 2A structure were performed with UCSF Chimera, developed by the Resource for Biocomputing, Visualization, and Informatics at the University of California, San Francisco.

Mutations that affected CV-B3 2A binding to SETD3 were annotated on the crystal structure in red. The (1-3)A mutations was not mapped to the structure as these mutations drastically affect protein stability. The four amino acids that constituted the ion coordination domain are annotated on the structure in blue. The three amino acids that formed the catalytic triad are annotated on the structure in pink.

Engineering of GFP-ΔVP1-2A constructs

The CVB3 GFP-2A plasmid was generated based on a previously published RV-B14 construct[56]. The RVB14 GFP-2A plasmid was a kind gift from Dr. Ann Palmenberg. The construct encodes an N-terminal GFP followed by partial RV-B14 VP1 C-terminal domain (ΔVP1, contains 2A *in cis* cleavage site), and 2A sequence. Transcription is driven by a CMV promoter followed by an EMCV IRES to allow for cap-independent translation of mRNA transcripts. The RV-B14 sequence was replaced by the similar sequences for CVB3 (35 a.a. of CV-B3 VP1 C-terminal domain that contains 2A *in cis* cleavage site and full 2A coding sequence). Indicated mutations in CV-B3 2A were incorporated using QuikChange Lightning Site-Directed Mutagenesis Kit (Agilent).

Engineering and expression of CV-B3-RLuc infectious RNA genomes that encode 2A mutations (fail to interact with SETD3)

The full-length CV-B3-RLuc infectious clone, pRLuc-53CB3/T7 (see *Viruses, reporter viruses, and infectious clones*), was used a template to introduce indicated triple-alanine substitutions in 2A using QuikChange Lightning Site-Directed Mutagenesis Kit (Agilent) or other standard cloning techniques. Engineered infectious cDNAs were then linearized with SmaI, purified, and transcribed using MEGAscript T7 Transcription Kit (Thermo Fisher). RNA was purified using RNeasy MinElute Cleanup Kit (Qiagen), and RNA quantity and quality was assessed using a Bioanalyzer 2100 RNA 6000 Nano Kit (Agilent). H1-HeLa WT cells (2×10^6) in electroporation buffer (Teknova) were electroporated with 2μg of the indicated purified viral RNAs using the square wave protocol (120V, 1.5ms pulse, 10 pulse, 1.5s interval, 1mm) on a Gene Pulser Xcell electroporator (Bio-Rad). Firefly luciferase mRNA was included as an electroporation control. Cells were plated in 96-well plates (5×10^4 cells/well) and were incubated for indicated time points. Cell lysates were harvested and luciferase signals were measured using the Renilla Luciferase Assay System (Promega) and a Veritas Microplate Luminometer (Turner).

Ethics statement and animal studies

All experiments involving mice were approved by Stanford's Institutional Animal Care and Use Committee (Administrative Panel of Laboratory Animal Care protocol #28856). Mice were housed in the Stanford University mouse facility, which is accredited by the Association for Assessment and Accreditation of Laboratory Animal Care International (AAALAC). Husbandry is performed in accordance with the Guide for the Care and Use of Laboratory Animals, 8th edition (2010) and the 2015 revision of the Public Health Service Policy on Humane Care and Use of Laboratory Animals. Room conditions included a temperature of 23°C, relative humidity of 30% to 40%, and a 12:12-h light:dark cycle (lights on, 0700 h). All mouse colonies are maintained under SPF conditions in irradiated disposable individually ventilated cages (InnocageR, Innovive, San Diego, CA) with

irradiated, corncob bedding, irradiated food (Teklad 2918 Global 18% Protein Rodent Diet, Envigo) and UV-irradiated, acidified (pH, 2.5 to 3.0), reverse-osmosis-purified bottled water (AquaviveR, Innovive). The mouse colonies are monitored for adventitious viral, bacterial, and parasitic pathogens by dirty-bedding sentinels. The sentinels are tested every 4 months and were found to be free of mouse parvovirus, minute virus of mice, mouse hepatitis virus, mouse rotavirus, Theiler's murine encephalomyelitis virus, murine norovirus, Sendai virus, mouse adenovirus 1 and 2, ectromelia virus, lymphocytic choriomeningitis virus, pneumonia virus of mice, respiratory enterovirus III, fur mites, lice, and pinworms. No statistical methods were used to predetermine sample size. In our animal study protocol, we state that the number of animals in each experimental group varies, and is based on a similar previous study[57]. Although pups were allocated to experimental groups randomly, once the genotypes were known the investigators were not blinded.

Mice

Two male and two female C57BL/6N - *Setd3*$^{tm1.1(NCOM)Mfgc}$/Tcp heterozygous mice were obtained from the Canadian Mouse Mutant Repository (CMMR, Toronto, Canada). The strain was made at the Toronto Centre for Phenogenomics as part of the NorCOMM2 project using NorCOMM ES cells[58]. Upon receipt the mice were mated and simultaneously crossed to C57BL/6NCrl females (Charles River Laboratories, Hollister, CA). Progeny were genotyped using either the Setd3-McKerlie PCR assay to identify either the 212-bp wild-type band (primers: Setd3_wt_F1-AACCAGCAGTGCACAGAGACAAGCTG; Setd3_wt_R1 - AACCCAAACTCTGCCAGCCAAAGCAC) and/or a 566 bp tm1.1 band (primers: Setd3_tm1_F4- AAACTGGTGCTGCTGATAACCTGGGC; GH717 - CACCGACGCCAATCACAAACAC) following instructions provided by the CMMR or the use of a commercial genotyping service (Transnetyx, Memphis, TN).

CV-A10, AV-A71, and EV-D68 infections in mice

For CV-A10 and EV-A71 infections, neonates at 2 days post-partum (P2) were inoculated intracerebrally into the left cerebral hemisphere under isoflurane general anesthesia. Pups were infected with either 1.5×10^5 PFU CV-A10 or 1.0×10^4 PFU EV-A71 in a volume of 1.0 μl using a 10 μl, gas tight, Hamilton syringe with a 33G needle[59]. Pups were allowed to recover on a heated pad then returned to their mother. For EV-D68 (MO), P2 pups were infected intramuscularly into the lateral aspect of the proximal left hindlimb[60] with 1.0 μl of 1.0×10^5 pfu EV-D68. Controls were injected similarly using uninfected RD cell tissue culture medium supernatant. Pups were allowed to recover on a heated pad then returned to their mother. Pups were toe tattooed for identification and a tip of tail removed for genotyping.

RNA Extraction from Mouse Tissues

Harvested tissues were weighed before homogenizing in Trizol reagent (Ambion) with 2.0mm RNase-free Zirconium Oxide Beads (Next Advance) in a Bullet Blender (Next Advance). In short, tissues were homogenized with three, 5-minute maximum speed runs at 4°C. Total RNA was then extracted and purified according to Trizol reagent manufacturer's guidelines (Ambion). Purified RNA was then reverse transcribed using iScript™ Reverse

Transcription Supermix for RT-qPCR (Bio-Rad) for qPCR quantification of viral RNA (see *Quantitation of virus infectivity by quantitative RT-PCR (qRT-PCR) section*).

Western blotting analysis

Cells were lysed in 2×Laemmli sample buffer (Bio-Rad) containing 5% beta-mercaptoethanol and incubated at 95°C for 10 minutes. Samples were separated by SDS-PAGE on pre-cast 4-15% poly-acrylamide gels (Bio-Rad) using Bio-rad Mini-PROTEAN gel system and transferred onto PVDF membranes (Bio-Rad). The PVDF membranes were blocked with 5% non-fat milk dissolved in 1×phosphate buffered saline (Corning) containing 0.1% Tween-20 (Sigma). Subsequently, membranes were incubated at 4°C for overnight with a primary antibody diluted in the blocking buffer. The following primary antibodies were used to detect the presence of indicated proteins in this study: SETD3 (Abcam, ab176582, 1:5000), SETD4 (antiserum from Dr. Or Gozani with 21st Century Biochemicals, 1:1000), SETD6 (Genetex, GTX629891, 1:10000), FLAG M2 (Sigma, F1804, 1:5000), P-84 (Genetex, GTX70220, 1:10000), GAPDH (GeneTex, GTX627408, 1:5000). After washing three times using PBS 0.1% Tween-20, membranes were incubated with secondary antibodies coupled to HRP (Genetex, GTX213111-01 (anti-mouse) or GTX213110-01 (anti-rabbit), 1:10000) for 1 hour at room temperature. Membranes were then washed three times before subjected to SuperSignal West Pico PLUS Chemiluminescent Substrate or Dura Extended Duration Substrate (Thermo Fisher) peroxide solutions treatment for visualization of antibody-bound proteins on film or Bio-Rad ChemiDoc Touch Imaging System.

Statistical analysis

GraphPad Prism 7 (GraphPad Software) was used to perform statistical analyses. The *P*-values for the mice survival curve were determined using the Log-rank (Mantel-Cox) test. Other *P*-values were determined by either two-tailed unpaired *t*-test, ordinary one-way ANOVA (Holm-Sidak corrected), or two-way ANOVA (Holm-Sidak corrected) on log-transformed data. ns = non-significant. * = $P < 0.05$. ** = $P < 0.0001$. Precise *P*-values are presented in Supplementary Table 6.

Data availability

Raw deep sequencing data corresponding to the CRISPR knockout screens reported in this paper are deposited in ArrayExpress (https://www.ebi.ac.uk/arrayexpress/) with accession number E-MTAB-8125.

Supplementary Material

Refer to Web version on PubMed Central for supplementary material.

Acknowledgements:

The authors would like to thank Carette laboratory members for intellectual discussions and support. We acknowledge Drs. Caleb Marceau (Chan Zuckerberg BioHub) and Andreas Puschnik (Chan Zuckerberg BioHub) for invaluable advice and technical assistance. We thank Drs. Karla Kirkegaard (Stanford University), Michael Holtzman (Washington University School of Medicine in St. Louis), Ann Palmenberg (University of Wisconsin-Madison), and Kevan Shokat (University of California San Francisco) for helpful discussions and valuable advice.

We express our gratitude to the Stanford shared FACS facility and its former director Marty Bigos, the Stanford Functional genomics facility and Xuhuai Ji, the Stanford University Mass Spectrometry Core and the SNAP team under guidance of Dr. Peter Jackson, the Stanford protein and nucleic acid facility, and the Stanford mouse facility for their excellent service and professional technical assistance. We thank Vincent Masto for technical assistance with cloning and Mike Shales for assistance preparing figures related to the mass spectrometry data. We acknowledge the NIH Biodefense and Emerging Infections Research Repository (BEI Resources), NIAID, NIH for providing multiple viruses mentioned in the *Materials and Methods*. We thank Dr. Jen-Ren Wang (National Cheng Kung University, Taiwan) for providing the EV-A71 (MP4) infectious clone. The work was funded in part by NSF GRFP (JD), Stanford Graduate Fellowship (JD), American Asthma Foundation 2014 Scholar Award (JEC), NIH DP2 AI104557 (JEC), NIH U19 AI109662 (JEC), NIH R01 AI140186 (JEC), Stanford Dean's Fellowship (YSO), David and Lucile Packard Foundation (JEC), NIH R01 GM079641 (OG), NIH P01-AI091575 (RA, NJK), NIH P50-GM082250 (NJK), NIH P50-GM081879 (NJK), NIH R01 AI021362 (HBG), NIH R56 AI021362 (HBG), VA Merit review grant GRH0022 (HBG), NIH K99 AI135031 (SD), Stanford Maternal & Child Health Research Institute (SD), and Thrasher Research Fund Early Career Award (SD).

References

1. Kaufmann SHE, Dorhoi A, Hotchkiss RS & Bartenschlager R Host-directed therapies for bacterial and viral infections. Nature reviews. Drug discovery 17, 35–56, doi:10.1038/nrd.2017.162 (2018). [PubMed: 28935918]
2. Bramley TJ, Lerner D & Sames M Productivity losses related to the common cold. Journal of occupational and environmental medicine 44, 822–829 (2002). [PubMed: 12227674]
3. Castillo JR, Peters SP & Busse WW Asthma Exacerbations: Pathogenesis, Prevention, and Treatment. The journal of allergy and clinical immunology. In practice 5, 918–927, doi:10.1016/j.jaip.2017.05.001 (2017). [PubMed: 28689842]
4. Palmenberg AC et al. Sequencing and analyses of all known human rhinovirus genomes reveal structure and evolution. Science (New York, N.Y.) 324, 55–59, doi:10.1126/science.1165557 (2009).
5. Cassidy H, Poelman R, Knoester M, Van Leer-Buter CC & Niesters HGM Enterovirus D68 - The New Polio? Frontiers in microbiology 9, 2677, doi:10.3389/fmicb.2018.02677 (2018). [PubMed: 30483226]
6. Bochkov YA et al. Cadherin-related family member 3, a childhood asthma susceptibility gene product, mediates rhinovirus C binding and replication. Proceedings of the National Academy of Sciences of the United States of America 112, 5485–5490, doi:10.1073/pnas.1421178112 (2015). [PubMed: 25848009]
7. Shalem O et al. Genome-scale CRISPR-Cas9 knockout screening in human cells. Science (New York, N.Y.) 343, 84–87, doi:10.1126/science.1247005 (2014).
8. Li W, Xu H, Xiao T, Cong L, Love MI, Zhang F, Irizarry RA, Liu JS, Brown M, Liu XS. MAGeCK enables robust identification of essential genes from genome-scale CRISPR/Cas9 knockout screens. Genome Biol. 2014;15(12):554. [PubMed: 25476604]
9. Liu Y et al. Sialic acid-dependent cell entry of human enterovirus D68. Nature communications 6, 8865, doi:10.1038/ncomms9865 (2015).
10. Hunt SL, Hsuan JJ, Totty N & Jackson RJ unr, a cellular cytoplasmic RNA-binding protein with five cold-shock domains, is required for internal initiation of translation of human rhinovirus RNA. Genes & development 13, 437–448 (1999). [PubMed: 10049359]
11. Staring J et al. PLA2G16 represents a switch between entry and clearance of Picornaviridae. Nature 541, 412–416, doi:10.1038/nature21032 (2017). [PubMed: 28077878]
12. Wilkinson AW et al. SETD3 is an actin histidine methyltransferase that prevents primary dystocia. Nature 565, 372–376, doi:10.1038/s41586-018-0821-8 (2019). [PubMed: 30626964]
13. Kwiatkowski S et al. SETD3 protein is the actin-specific histidine N-methyltransferase. eLife 7, doi:10.7554/eLife.37921 (2018).
14. Messacar K et al. Enterovirus D68 and acute flaccid myelitis-evaluating the evidence for causality. The Lancet. Infectious diseases, doi:10.1016/s1473-3099(18)30094-x (2018).
15. Chen K et al. Methyltransferase SETD2-Mediated Methylation of STAT1 Is Critical for Interferon Antiviral Activity. Cell 170, 492–506.e414, doi:10.1016/j.cell.2017.06.042 (2017). [PubMed: 28753426]

16. Wang C et al. The methyltransferase NSD3 promotes antiviral innate immunity via direct lysine methylation of IRF3. The Journal of experimental medicine 214, 3597–3610, doi:10.1084/jem.20170856 (2017). [PubMed: 29101251]
17. Lamphear BJ et al. Mapping the cleavage site in protein synthesis initiation factor eIF-4 gamma of the 2A proteases from human Coxsackievirus and rhinovirus. The Journal of biological chemistry 268, 19200–19203 (1993). [PubMed: 8396129]
18. Verschueren E et al. Scoring Large-Scale Affinity Purification Mass Spectrometry Datasets with MiST. Current protocols in bioinformatics 49, 8.19.11–16, doi:10.1002/0471250953.bi0819s49 (2015).
19. Watters K & Palmenberg AC Differential processing of nuclear pore complex proteins by rhinovirus 2A proteases from different species and serotypes. Journal of virology 85, 10874–10883, doi:10.1128/jvi.00718-11 (2011). [PubMed: 21835805]
20. Ventoso I, MacMillan SE, Hershey JW & Carrasco L Poliovirus 2A proteinase cleaves directly the eIF-4G subunit of eIF-4F complex. FEBS letters 435, 79–83 (1998). [PubMed: 9755863]
21. Greninger AL, Knudsen GM, Betegon M, Burlingame AL & Derisi JL The 3A protein from multiple picornaviruses utilizes the golgi adaptor protein ACBD3 to recruit PI4KIIIbeta. Journal of virology 86, 3605–3616, doi:10.1128/jvi.06778-11 (2012). [PubMed: 22258260]
22. Wessels E et al. A viral protein that blocks Arf1-mediated COP-I assembly by inhibiting the guanine nucleotide exchange factor GBF1. Developmental cell 11, 191–201, doi:10.1016/j.devcel.2006.06.005 (2006). [PubMed: 16890159]
23. Torres JZ, Miller JJ & Jackson PK High-throughput generation of tagged stable cell lines for proteomic analysis. Proteomics 9, 2888–2891, doi:10.1002/pmic.200800873 (2009). [PubMed: 19405035]
24. Petersen JF et al. The structure of the 2A proteinase from a common cold virus: a proteinase responsible for the shut-off of host-cell protein synthesis. The EMBO journal 18, 5463–5475, doi:10.1093/emboj/18.20.5463 (1999). [PubMed: 10523291]
25. Yu SF & Lloyd RE Characterization of the roles of conserved cysteine and histidine residues in poliovirus 2A protease. Virology 186, 725–735 (1992). [PubMed: 1310193]
26. Dickinson ME et al. High-throughput discovery of novel developmental phenotypes. Nature 537, 508–514, doi:10.1038/nature19356 (2016). [PubMed: 27626380]
27. Huang PN & Shih SR Update on enterovirus 71 infection. Current opinion in virology 5, 98–104, doi:10.1016/j.coviro.2014.03.007 (2014). [PubMed: 24727707]
28. Li S et al. A neonatal mouse model of coxsackievirus A10 infection for anti-viral evaluation. Antiviral research 144, 247–255, doi:10.1016/j.antiviral.2017.06.008 (2017). [PubMed: 28625478]
29. Huang SW, Wang YF, Yu CK, Su IJ & Wang JR Mutations in VP2 and VP1 capsid proteins increase infectivity and mouse lethality of enterovirus 71 by virus binding and RNA accumulation enhancement. Virology 422, 132–143, doi:10.1016/j.virol.2011.10.015 (2012). [PubMed: 22078110]
30. Hambidge SJ & Sarnow P Translational enhancement of the poliovirus 5' noncoding region mediated by virus-encoded polypeptide 2A. Proceedings of the National Academy of Sciences of the United States of America 89, 10272–10276 (1992). [PubMed: 1332040]
31. Li X, Lu HH, Mueller S & Wimmer E The C-terminal residues of poliovirus proteinase 2A(pro) are critical for viral RNA replication but not for cis- or trans-proteolytic cleavage. The Journal of general virology 82, 397–408, doi:10.1099/0022-1317-82-2-397 (2001). [PubMed: 11161279]
32. Lloyd RE, Grubman MJ & Ehrenfeld E Relationship of p220 cleavage during picornavirus infection to 2A proteinase sequencing. Journal of virology 62, 4216–4223 (1988). [PubMed: 2845133]
33. Ryan MD & Flint M Virus-encoded proteinases of the picornavirus super-group. The Journal of general virology 78 (Pt 4), 699–723, doi:10.1099/0022-1317-78-4-699 (1997). [PubMed: 9129643]
34. Hoshii T et al. A Non-catalytic Function of SETD1A Regulates Cyclin K and the DNA Damage Response. Cell 172, 1007–1021.e1017, doi:10.1016/j.cell.2018.01.032 (2018). [PubMed: 29474905]

35. Lai AC & Crews CM Induced protein degradation: an emerging drug discovery paradigm. Nature reviews. Drug discovery 16, 101–114, doi:10.1038/nrd.2016.211 (2017). [PubMed: 27885283]
36. Lanke KH et al. GBF1, a guanine nucleotide exchange factor for Arf, is crucial for coxsackievirus B3 RNA replication. Journal of virology 83, 11940–11949, doi:10.1128/jvi.01244-09 (2009). [PubMed: 19740986]
37. Bochkov YA et al. Molecular modeling, organ culture and reverse genetics for a newly identified human rhinovirus C. Nature medicine 17, 627–632, doi:10.1038/nm.2358 (2011).
38. Sanjana NE, Shalem O & Zhang F Improved vectors and genome-wide libraries for CRISPR screening. Nature methods 11, 783–784, doi:10.1038/nmeth.3047 (2014). [PubMed: 25075903]
39. Marceau CD et al. Genetic dissection of Flaviviridae host factors through genome-scale CRISPR screens. Nature 535, 159–163, doi:10.1038/nature18631 (2016). [PubMed: 27383987]
40. Verstrepen WA, Kuhn S, Kockx MM, Van De Vyvere ME & Mertens AH Rapid detection of enterovirus RNA in cerebrospinal fluid specimens with a novel single-tube real-time reverse transcription-PCR assay. Journal of clinical microbiology 39, 4093–4096, doi:10.1128/jcm.39.11.4093-4096.2001 (2001). [PubMed: 11682535]
41. Bragstad K et al. High frequency of enterovirus D68 in children hospitalised with respiratory illness in Norway, autumn 2014. Influenza and other respiratory viruses 9, 59–63, doi:10.1111/irv.12300 (2015). [PubMed: 25534826]
42. McKnight KL & Lemon SM Capsid coding sequence is required for efficient replication of human rhinovirus 14 RNA. Journal of virology 70, 1941–1952 (1996). [PubMed: 8627720]
43. Ding S et al. Comparative Proteomics Reveals Strain-Specific beta-TrCP Degradation via Rotavirus NSP1 Hijacking a Host Cullin-3-Rbx1 Complex. PLoS pathogens 12, e1005929, doi:10.1371/journal.ppat.1005929 (2016). [PubMed: 27706223]
44. Cox J & Mann M MaxQuant enables high peptide identification rates, individualized p.p.b.-range mass accuracies and proteome-wide protein quantification. Nature biotechnology 26, 1367–1372, doi:10.1038/nbt.1511 (2008).
45. Kron SJ, Drubin DG, Botstein D & Spudich JA Yeast actin filaments display ATP-dependent sliding movement over surfaces coated with rabbit muscle myosin. Proceedings of the National Academy of Sciences of the United States of America 89, 4466–4470 (1992). [PubMed: 1533933]
46. Schafer DA, Jennings PB & Cooper JA Rapid and efficient purification of actin from nonmuscle sources. Cell motility and the cytoskeleton 39, 166–171, doi:10.1002/(sici)1097-0169(1998)39:2<166::Aid-cm7>3.0.Co;2-4 (1998). [PubMed: 9484958]
47. Ramage HR et al. A combined proteomics/genomics approach links hepatitis C virus infection with nonsense-mediated mRNA decay. Molecular cell 57, 329–340, doi:10.1016/j.molcel.2014.12.028 (2015). [PubMed: 25616068]
48. Clauser KR, Baker P & Burlingame AL Role of accurate mass measurement (+/− 10 ppm) in protein identification strategies employing MS or MS/MS and database searching. Analytical chemistry 71, 2871–2882 (1999). [PubMed: 10424174]
49. Duke GM, Hoffman MA & Palmenberg AC Sequence and structural elements that contribute to efficient encephalomyocarditis virus RNA translation. Journal of virology 66, 1602–1609 (1992). [PubMed: 1310768]
50. Jager S et al. Global landscape of HIV-human protein complexes. Nature 481, 365–370, doi:10.1038/nature10719 (2011). [PubMed: 22190034]
51. Jager S et al. Purification and characterization of HIV-human protein complexes. Methods (San Diego, Calif.) 53, 13–19, doi:10.1016/j.ymeth.2010.08.007 (2011).
52. Choi H et al. SAINT: probabilistic scoring of affinity purification-mass spectrometry data. Nature methods 8, 70–73, doi:10.1038/nmeth.1541 (2011). [PubMed: 21131968]
53. Choi H et al. Analyzing protein-protein interactions from affinity purification-mass spectrometry data with SAINT. Current protocols in bioinformatics Chapter 8, Unit8.15, doi:10.1002/0471250953.bi0815s39 (2012).
54. MacLean B et al. Skyline: an open source document editor for creating and analyzing targeted proteomics experiments. Bioinformatics (Oxford, England) 26, 966–968, doi:10.1093/bioinformatics/btq054 (2010).

55. Choi M et al. MSstats: an R package for statistical analysis of quantitative mass spectrometry-based proteomic experiments. Bioinformatics (Oxford, England) 30, 2524–2526, doi:10.1093/bioinformatics/btu305 (2014).

56. Watters K et al. Differential Disruption of Nucleocytoplasmic Trafficking Pathways by Rhinovirus 2A Proteases. Journal of virology 91, doi:10.1128/jvi.02472-16 (2017).

57. Mao Q et al. A neonatal mouse model of coxsackievirus A16 for vaccine evaluation. Journal of virology 86, 11967–11976, doi:10.1128/jvi.00902-12 (2012). [PubMed: 22951825]

58. Bradley A et al. The mammalian gene function resource: the International Knockout Mouse Consortium. Mammalian genome : official journal of the International Mammalian Genome Society 23, 580–586, doi:10.1007/s00335-012-9422-2 (2012). [PubMed: 22968824]

59. Li J & Daly TM Adeno-associated virus-mediated gene transfer to the neonatal brain. Methods (San Diego, Calif.) 28, 203–207 (2002).

60. Hixon AM et al. A mouse model of paralytic myelitis caused by enterovirus D68. PLoS pathogens 13, e1006199, doi:10.1371/journal.ppat.1006199 (2017). [PubMed: 28231269]

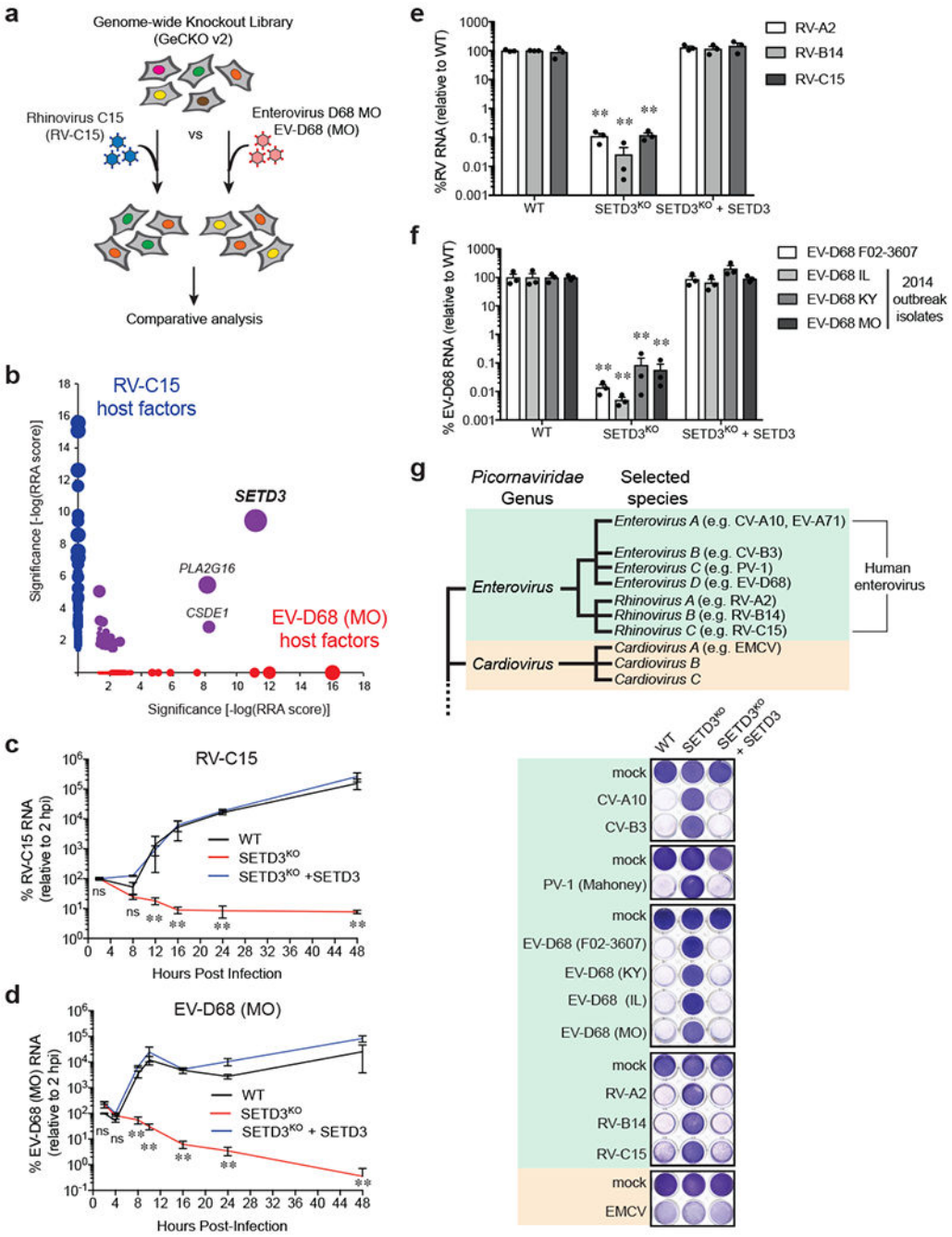

Figure 1. Genome-wide CRISPR-Cas9 screens identify SETD3 as a broad host factor for human enteroviruses.

a, Diagram for genome-wide CRISPR-Cas9 knockout screening approach. A library of CRISPR-Cas9 knockout cells was infected with either rhinovirus C15 (RV-C15) or enterovirus D68 Missouri (EV-D68 MO) and cells resistant to viral infection were selected. Genes enriched for both viruses were then compared. **b,** Combined plot of RV-C15 (blue, y-axis) and EV-D68 MO (red, x-axis) CRISPR-Cas9 screen results. $n = 1$ for each screen. Significance of enrichment was calculated by MAGeCK analysis. Genes enriched in both

screens are indicated in purple. **c-f,** qRT-PCR quantification of RV and EV-D68 RNA in infected wild-type (WT), SETD3 knockout ($SETD3^{KO}$), and SETD3 stably complemented ($SETD3^{KO}$ + SETD3) H1-HeLa cell lines over time (**c** and **d**) and at 16 hpi (**e** and **f**). For panel **c**, **d**, **e**, and **f**, datasets represent the mean with standard error of the mean (SEM) of $n = 3$ independent biological replicates. All *P*-values were determined by two-way ANOVA (Holm-Sidak corrected) on log-transformed data using GraphPad Prism (GraphPad Software). ns = non-significant. * = $P < 0.05$. ** = $P < 0.0001$. Precise *P*-values are presented in Supplementary Table 6. **g,** Top panel, classification and examples of *Enterovirus* (highlighted in green) and *Cardiovirus* (highlighted in orange). Bottom panel, crystal violet staining of viable cells after infection with indicated picornaviruses. mock, uninfected control. Representative crystal violet viability staining of $n = 3$ biologically independent replicates showing similar results.

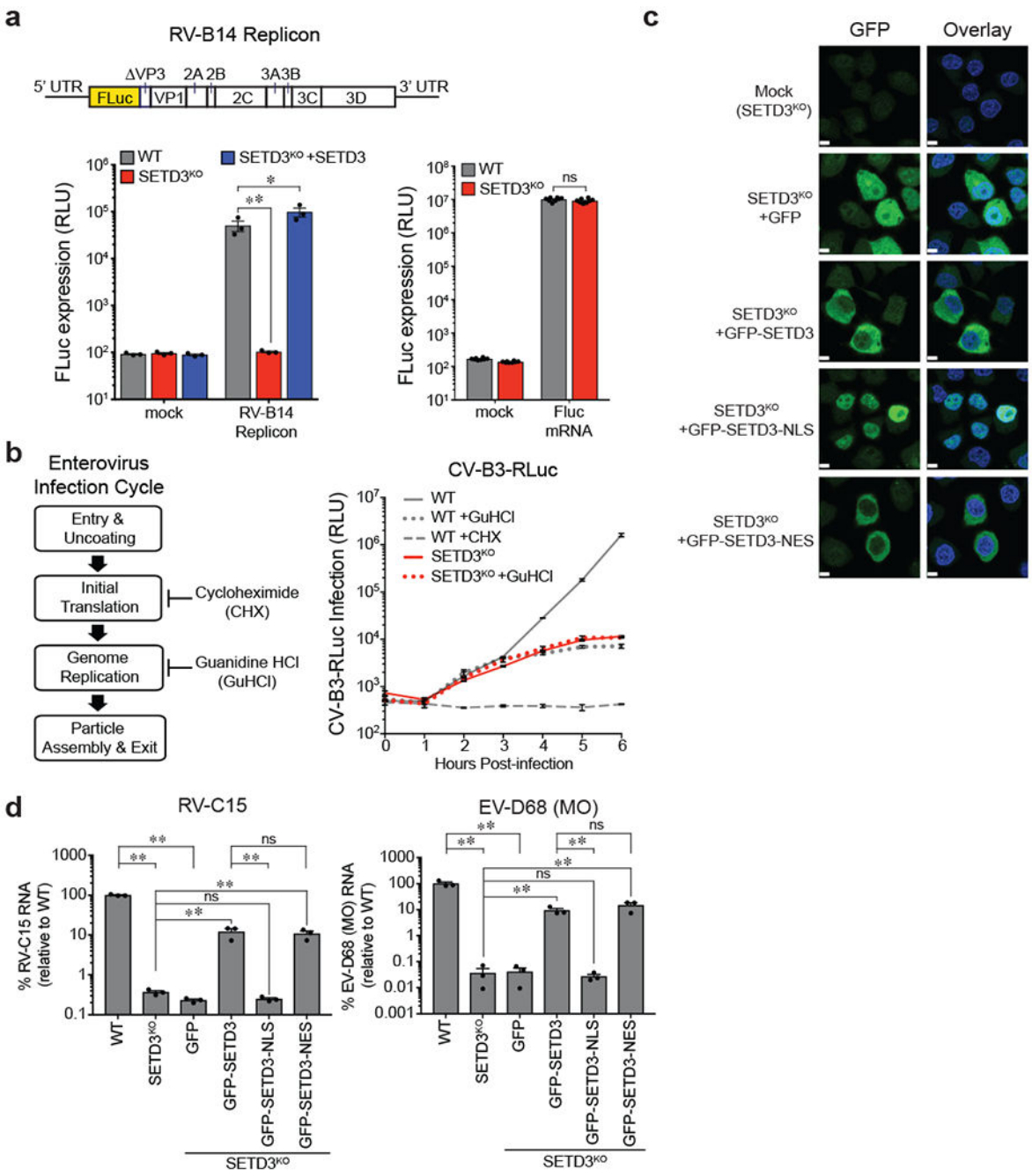

Figure 2. SETD3 is required for enterovirus replication in the cytoplasm.

a, RV-B14 replicon or firefly luciferase mRNA control luciferase expression in wild-type (WT; H1-HeLa^{+CDHR3}), SETD3 knockout (SETD3^{KO}), and SETD3 stably complemented (SETD3^{KO} + SETD3 cDNA) cell lines. Top panel is a schematic for RV-B14 replicon construct, in which Firefly luciferase reporter gene (FLuc) was inserted to replace the majority of the structural proteins **b,** Schematic for enterovirus infection cycle and inhibitors that block specific stages during viral infection are indicated. Synchronized luciferase-expressing CV-B3 infection of SETD3^{KO} cells and WT cells treated with either 125 μM

cycloheximide (CHX) or 2 mM guanidine hydrochloride (GuHCl) over a time course (right panel). **c,** Confocal imaging of $SETD3^{KO}$ cells and $SETD3^{KO}$ cells that stably expressed GFP, SETD3 fused with GFP at the N-terminal (GFP-SETD3), GFP-SETD3 fused with a nuclear localization signal (GFP-SETD3-NLS), or GFP-SETD3 fused with a nuclear export signal (GFP-SETD3-NES). A representative set of two independent experiments is shown here. Scale bars, 7 μm. **d,** qRT-PCR quantification of viral RNA levels in RV-C15 or EV-D68 MO infected cell lines. All of the complemented constructs were expressed under a minimal expression promoter. For panel **a**, **b**, and **d,** datasets represent the mean with SEM of $n = 3$ independent biological replicates. *P*-values were determined by either two-way ANOVA (**a** and **b**) or ordinary one-way ANOVA (**d**) with Holm-Sidak correction on log-transformed data. For panel **b**, at 4 hpi and beyond, all differences observed between untreated WT vs. all other conditions are statistically significant ($P < 0.0001$). ns = non-significant. * = $P < 0.05$. ** = $P < 0.0001$.

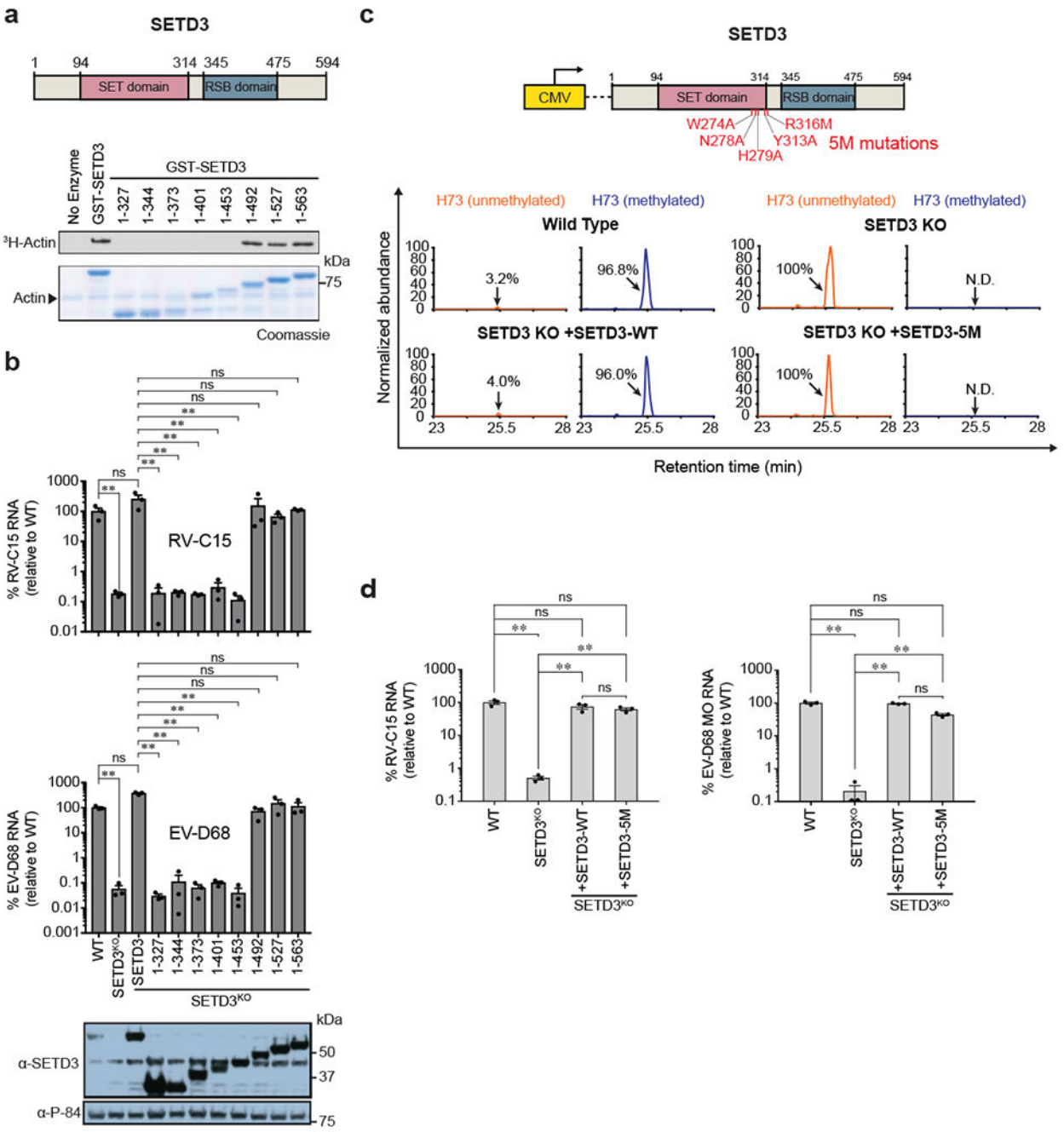

Figure 3. The SET and RSB domain of SETD3 are required for its role in viral replication but not its methyltransferase activity.

a, *In vitro* methylation assay of actin with indicated GST-SETD3 C-terminal truncation mutants. Top panel is a schematic for SETD3 protein, which contains a SET domain and a Rubisco substrate binding (RSB) domain. Middle panel shows detection of methylation of actin at residue H73 by radioactivity. Expression of SETD3 truncation mutants is shown by Coomassie staining on the bottom panel. **b,** qRT-PCR quantification of viral RNA levels of RV-C15 (top panel) and EV-D68 MO (middle panel) infected cells in WT, SETD3^{KO}, and

SETD3^{KO} stably complemented with SETD3 truncation mutants. Expression of SETD3 truncation mutants is shown by western blot on the bottom panel. Representative western blot of $n = 2$ biologically independent replicates showing similar results. **c,** Chromatograms for quantification of actin H73 methylation by tandem MS/MS using cell lysates from WT cells, SETD3^{KO} cells, or SETD3^{KO} cells stably expressing wild type SETD3 cDNA (SETD3-WT) or catalytically inactive SETD3 cDNA containing 5 mutations (SETD3-5M). All of the complemented cDNA constructs were expressed under a high-expression promoter (CMV). The area of indicated peaks was normalized to the sum area between peptides (± methylation) and percent abundance is labeled. N.D. not detected. Top panel is a schematic of SETD3 with the 5 mutations (W274, N278, H279 Y313, and R316) indicated. **d,** qRT-PCR quantification of viral RNA levels in RV-C15 or EV-D68 MO infected cell lines described in panel **c**. For panel **a** and **c**, data are representative of three independent biological replicates with similar results. qRT-PCR datasets shown in panel **b** and **d** represent the mean with SEM of $n = 3$ independent biological replicates. *P*-values were determined by ordinary one-way ANOVA (Holm-Sidak corrected) on log-transformed data. ns = non-significant. * = $P < 0.05$. ** = $P < 0.0001$.

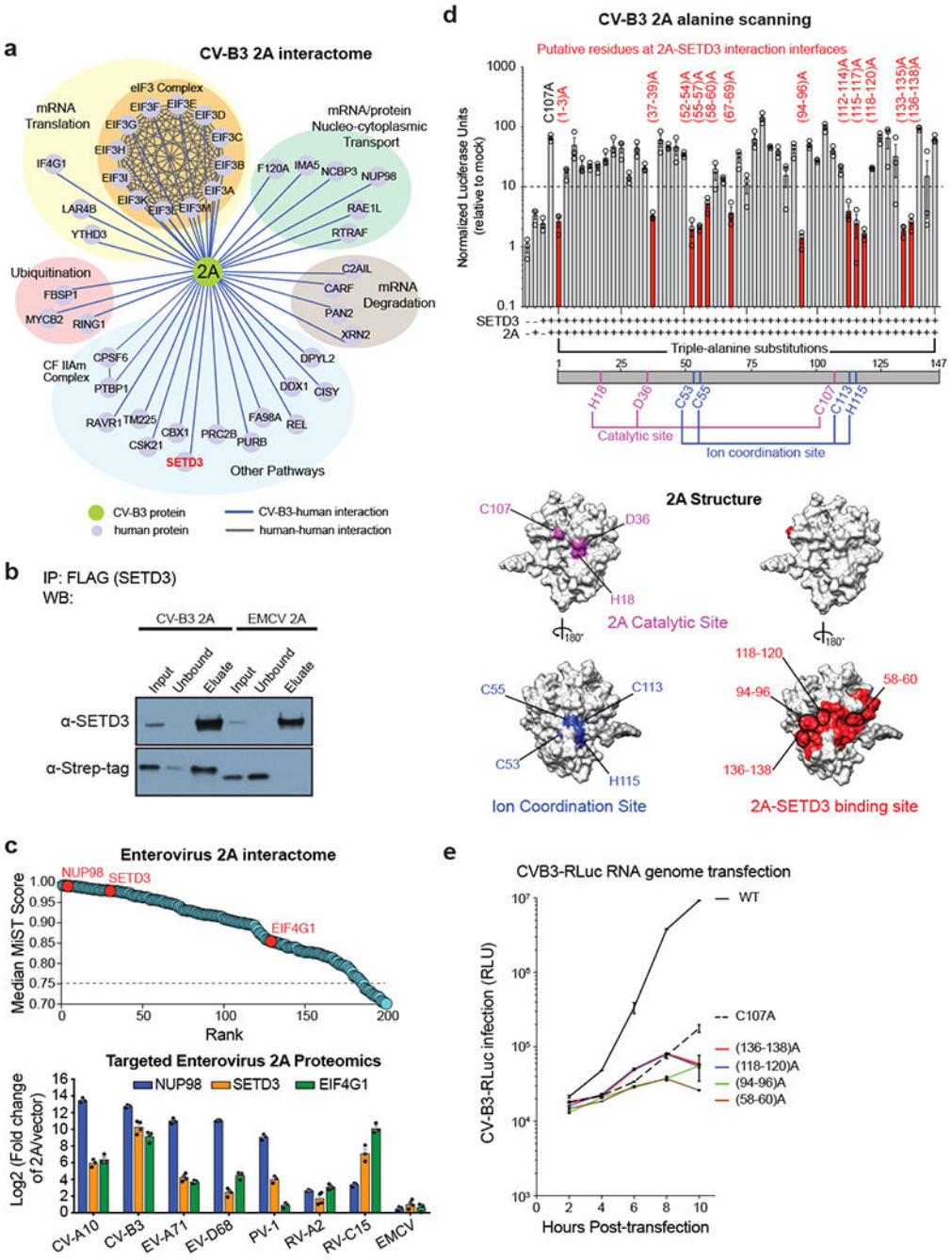

Figure 4. SETD3 interacts with enteroviral 2A protein to promote viral replication.

a, High-confidence CV-B3 2A-interacting host proteins with a MiST score > 0.75 in a comprehensive CV-B3-host protein-protein interaction map generated using affinity tag-purification mass spectrometry (AP-MS). Proteins are grouped into complexes and pathways. Highlighted in red, SETD3. **b,** Immunoprecipitation-western blot (IP-WB) of cells transfected with FLAG-SETD3 and CV-B3 2A-Strep. Unrelated EMCV 2A-Strep was used as control. Representative IP-WB of $n = 2$ biologically independent replicates showing similar results. **c,** AP-MS of cells expressing 2A proteins from a panel of indicated

enteroviruses (7 in total). Upper panel, median MiST scores of these 7 affinity purifications. Top 200 hits are ranked along the x-axis. Cutoff median MiST score of 0.75 indicated by dotted line. Labeled and highlighted in red: NUP98, SETD3, and EIF4G1. Bottom panel, enrichment of NUP98, SETD3, and EIF4G1 intensity (over control) in affinity purifications of the individual enterovirus 2A proteins measured by targeted proteomics. Data represent the mean with SEM of $n = 4$ independent biological replicates, except for CV-A10, PV-1 and RV-C15 ($n = 3$). **d**, Alanine scanning characterization of protein-protein interactions between 2A and SETD3 using the CheckMate mammalian two-hybrid system. Red, 2A mutations that disrupted 2A-SETD3 interaction (< 10-fold activation). 2-dimensional schematic and 3-dimensional structure of 2A: purple, known catalytic residues; blue, highly conserved residues that coordinate ion binding; red, putative 2A residues involved in SETD3 binding. Labeled and circled, four mutants tested in **e**. **e,** Replication kinetics of CV-B3-RLuc RNA in wild-type H1-HeLa cells. Cells were transfected with full-length wild-type virus RNA, a mutant that harbored the $2A^{C107A}$ catalytic mutation, or mutants that carried the indicated 2A mutations (failed to interact with SETD3) without the C107A catalytic mutation. For panels **d** and **e**, data represent the mean with SEM of $n = 3$ independent biological replicates. *P*-values calculated by either ordinary one-way ANOVA (**d**) or two-way ANOVA with Holm-Sidak correction on log-transformed data (**e**). For panel **d**, all mutants with markedly disrupted SETD3 interaction (< 10-fold activation; red) have a statistically significant reduction in activation compared to $2A^{C107A}$ control ($P < 0.0001$). For panel **e**, at 4 hpi and beyond, the differences observed between WT and all other mutants are statistically significant ($P < 0.0001$).

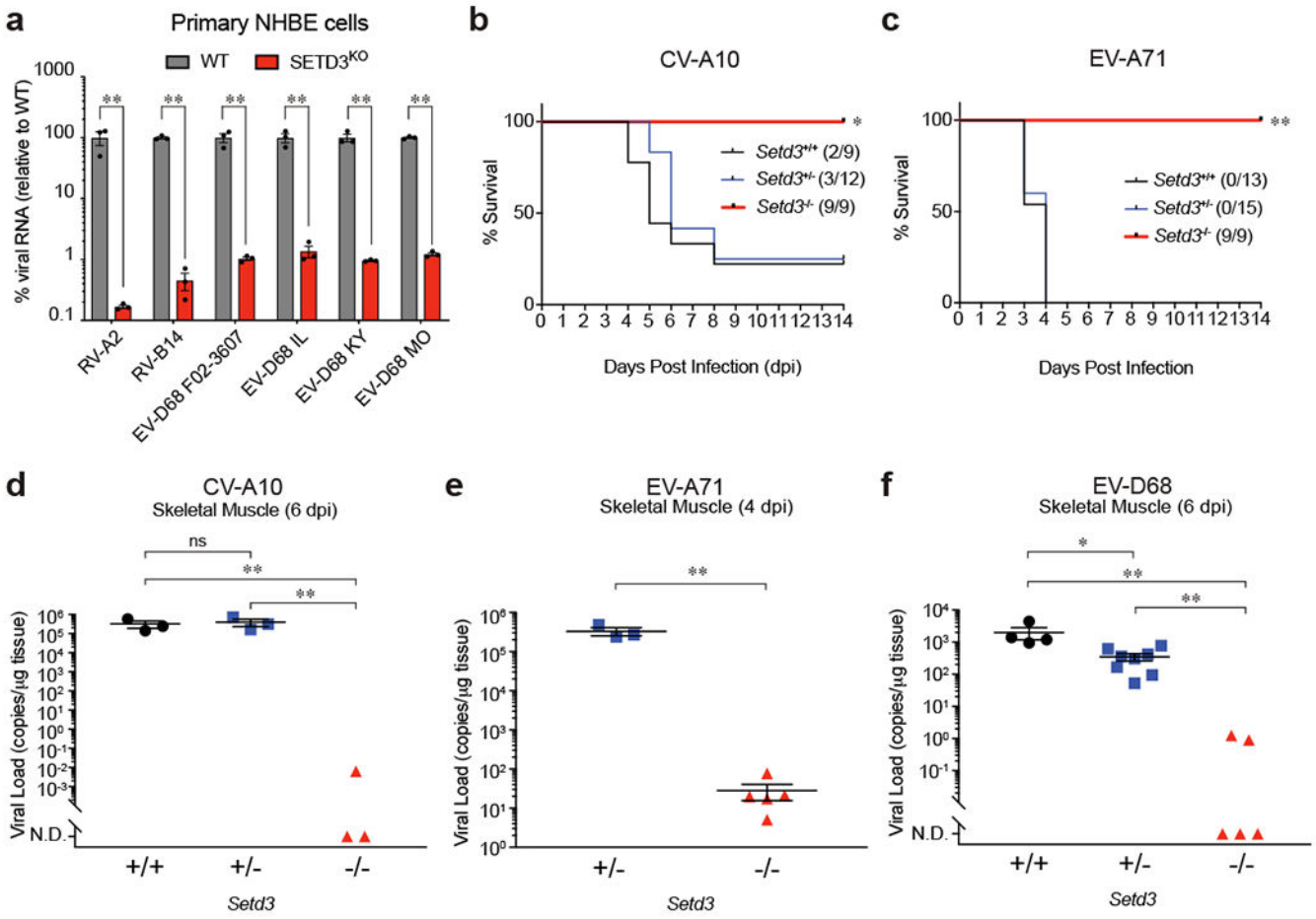

Figure 5. SETD3 is important for enterovirus infection of primary human cells and *in vivo* mouse models.

a, qRT-PCR quantification of viral RNA levels of RV-A2, RV-B14 and multiple EV-D68 strains infected human primary normal bronchial epithelial (NHBE) cells and SETD3^{KO} NHBE cells. Datasets represent the mean with SEM of $n = 3$ independent biological replicates. **b,** Survival curve for wild-type (*Setd3*$^{+/+}$), heterozygous (*Setd3*$^{+/-}$), and homozygous SETD3 knockout (*Setd3*$^{-/-}$) mice injected intracerebrally with coxsackievirus A10 (CV-A10) at 150,000 infectious particles/mouse. **c**, Survival curve for mice injected intracerebrally with enterovirus A71 (EV-A71) at 10,000 infectious particles/mouse. For panels **b** and **c**, the number of survivors over the total number for each group of mice is indicated in parenthesis. **d,** qRT-PCR quantification of viral RNA levels of CV-A10 present in the hind-limb skeletal muscle at 6 dpi of indicated mice. Data represents the mean with SEM of $n = 3$ animals for each group of mice. **e,** qRT-PCR quantification of viral RNA levels of EV-A71 present in the hind-limb skeletal muscle at 4 dpi of indicated mice. Data represents the mean with SEM of $n = 3$ (*Setd3*$^{+/+}$) or $n = 5$ (*Setd3*$^{+/-}$) mice. **f,** qRT-PCR quantification of viral RNA levels of enterovirus D68 (EV-D68) at 6 dpi in mice injected intramuscularly with 100,000 infectious particles/mouse at 6 dpi. Data represents the mean with SEM of $n = 4$ (*Setd3*$^{+/+}$), $n = 8$ (*Setd3*$^{+/-}$) or $n = 5$ (*Setd3*$^{-/-}$) mice. For panel **a**, **d**, and **f**, *P*-values were determined by either two-way ANOVA (**a**), ordinary one-way ANOVA (**d**

and **f**) with Holm-Sidak correction on log-transformed data. For panel **b** and **c**, Two-tailed *P*-values for survival of *Setd3*$^{-/-}$ mice versus wild type were determined by log-rank (Mantel-Cox) test. For panel **e**, *P*-values were determined by two-tailed unpaired t-test on log-transformed data. ns = non-significant. * = $P < 0.05$. ** = $P < 0.0001$.